THE RESPONSE OF RAILROAD WHEELS TO CONTINUOUS EXCITATION AND IMPACT

A Thesis

Presented to

the Faculty of the Department of Mechanical Engineering

University of Houston

In Partial Fulfillment

of the Requirements for the Degree

Master of Science

---

by

Kornel Nagy

May, 1971

To

My Wife, Joan

ACKNOWLEDGEMENTS

The author would like to express his sincere appreciation to the following:

Dr. R. D. Finch, his advisor, who provided assistance, encouragement, and counsel throughout his graduate study program.

Mr. J. O. Beauchamp for his cooperation and assistance in sharing the same electronic equipment.

Mr. B. Smith and Mr. J. Baklik for manufacturing the model wheels.

Mr. D. DeGeorge for his assistance with the instrumentation.

His wife, Joan, his sons, Chris and Tony, his daughters, Julie, Sandra, and Nancy, whose faith and encouragement never ceases.

THE RESPONSE OF RAILROAD WHEELS
TO CONTINUOUS EXCITATION AND IMPACT

An Abstract of a Thesis
Presented to
the Faculty of the Department of Mechanical Engineering
University of Houston

In Partial Fulfillment
of the Requirements for the Degree
Master of Science

---

by
Kornel Nagy
May, 1971

ABSTRACT

The responses of 1/4 scale model railroad wheels to continuous excitation and impact were investigated. Good wheels as well as wheels with cracks were tested on test stands inside an anechoic chamber.

It was found that wheels with cracks can be detected by the analysis of the airborne sound that is emitted when the wheel resonances are sufficiently excited. The method of detection is on a comparative basis by matching the resonances of good wheels against the resonances of the wheel under test.

The experiments showed that 50 kHz bandwidth continuous random noise excitation produces better comparative results than impact excitation.

TABLE OF CONTENTS

LIST OF SYMBOLS

a	outer radius of annular plate
b	inner radius of annular plate
C_n	constant
D	flexural rigidity of plate
D_n	constant
E	Young's modulus
E_n	constant
f_{nm}	frequency
F_n	constant
g	acceleration due to gravity
H	thickness of plate
I	moment of inertia
J_n	Bessel function of the first kind of order n
k,m,n	integers
p	lateral force per unit area on plate
P	coordinate point on plate
r,R	radius of circle
t	time
w,W	displacement
x,y,z	cartesian coordinates
Y_n	Bessel function of the second kind of order n

....

β	constant
γ	specific weight

∇^2	Laplacian operator
δ_{om}	eigenvalues for the symmetric modes
θ, Θ	angle in general
λ_{no}	eigenvalues for the asymmetric modes
ν	Poisson's ratio
ρ_x, ρ_y	radius of curvature, in the x and y directions
ϕ_x, ϕ_y	angle in general
ω	constant, angular frequency

LIST OF TABLES

LIST OF FIGURES

Chapter 1

INTRODUCTION

1.1 Statement of the Problem

Defective railroad wheels (See Figure 1.1) are one of the primary causes of train derailments, expensive in terms of property losses, injuries, loss of life and replacement costs. The need exists for finding defective wheels and removing them from service prior to failure. To date there is no effective test program capable of monitoring all railroad wheels.

In the development of such a program the following should be considered:

a. The rolling stock of the railroads is dispersed throughout the country. Any program that is implemented should test a maximum number of wheels, with a minimum number of test stations.

b. The wheels in use today vary in size, age and method of manufacture,[1] so the test equipment that is developed must be able to monitor wheels of all sizes, ages and manufacture.

c. The defects that develop may occur on any part of the wheel. The defects are of different types, and are caused by different mechanisms. As a result their growth rates, location and their effect on the operation of the wheel are varied. The ideal test equipment should differentiate between failure types, and

[1]Bray [1] and Dalvi [2] have presented discussions of the various wheel types and manufacturing methods and types of defect.

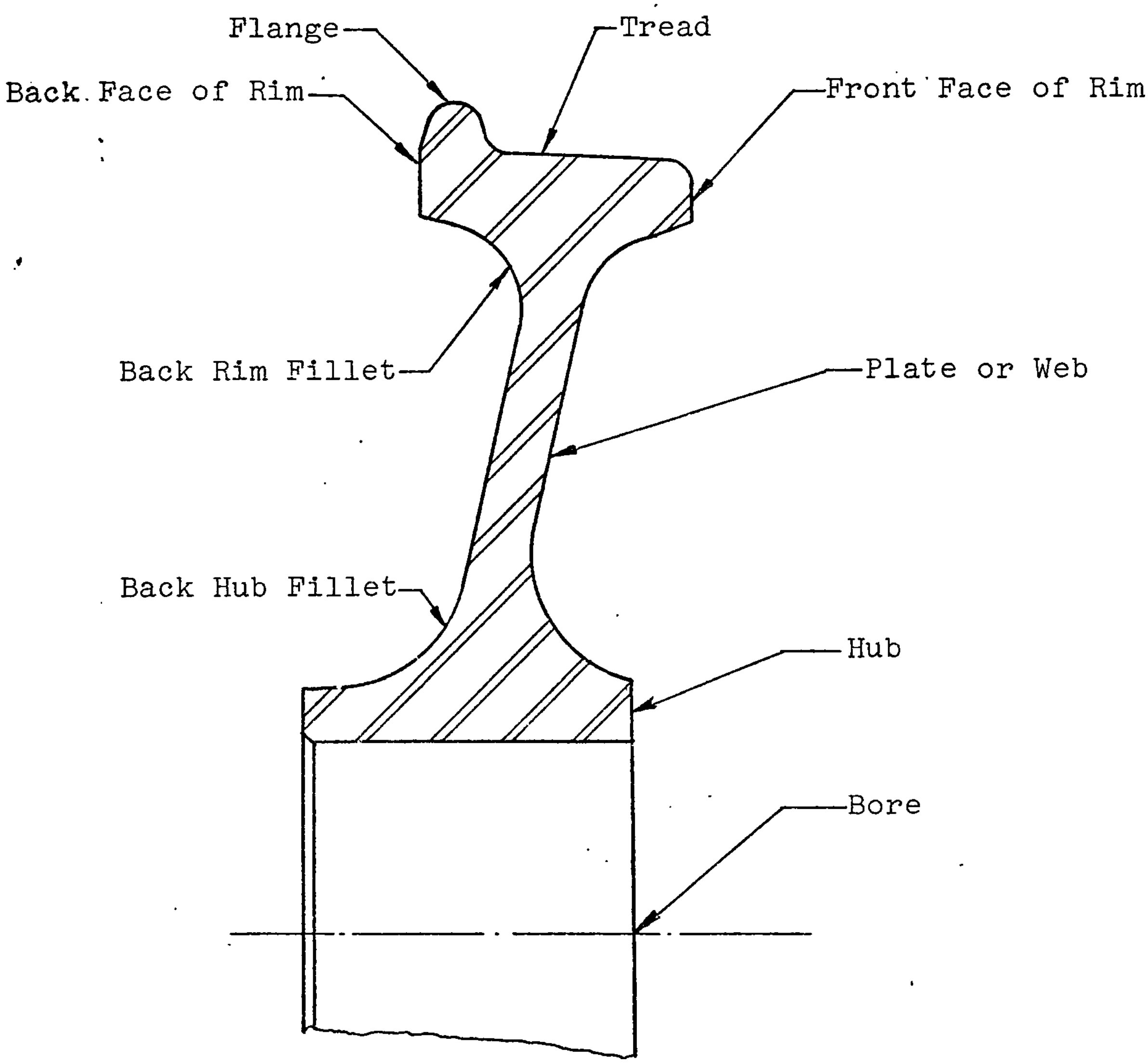

Fig. 1.1 Railroad Wheel Nomenclature

provide approximate information of time to failure.

d. Ideally the wheels should be tested in service. This is an important requirement, because if service must be interrupted for testing the wheels, the test program costs could run in excess of any losses incurred from wheel failure.

1.2 Current Testing Methods

All non destructive wheel testing methods that are currently in use are crack detection methods [2]. A crack, void or a broken out portion of the wheel is detected by visual inspection, eddy current inspection, or ultrasonic inspection. In the visual inspection method the cracks are shown up by the use of various penetrants which when viewed under ultraviolet light outline the cracks. This testing method is well suited to production line testing in wheel manufacturing, but cannot be readily used for in service testing.

Presently eddy current testing methods are under development. In this approach a coil is placed close to the tread of the wheel, and an alternating current is passed through the coil. The eddy currents induced by the coil permeate the tread surface. Cracks and discontinuities if present impede the circulation of these currents and as a result the power consumption of the detection coil will decrease. This is observed as a change in the current flowing through the coil. This method appears promising, however it has limited penetration depth and can only monitor the treads of the wheel. The application of this method to a moving train is severly limited by the fact that each wheel would require a separate detection coil. Current applications involve monitoring of diesel locomotive wheels, where adequate power is available to supply the associated electronics.

Ultrasonic crack detection methods are widely used in industry.[1,2] Various inspection methods have been developed to suit the testing requirements of a wide variety of products. In this detection method an ultrasonic pulse is sent into the part and discontinuities show up as so called pulse echoes. Ultrasonic testing of wheels is routinely done in the manufacture of wheels. However, to date ultrasonic testing of wheels on moving trains has not been realized. The technique is used only for the rim at the present time and the wheel must be scanned over its entire surface.

Recent work by Bray and Dalvi brought forth very promising results that may aid in the development of an ultrasonic test method for moving wheels. Bray's initial investigation showed that if ultrasonic pulses were generated on the tread, waves would travel both through the rim and plate regions. He also found that surface waves propagating circumferentially along the tread were very strong. Dalvi investigated these surface waves in the tread and found that they were indeed suitable for the detection of thermal cracks on the tread. A significant point of their work is that the ultrasonic probe was applied to the wheel at the same point where the wheel contacts the railroad track during normal operation. Bray[3] is currently investigating the propagation of ultrasonic pulses through the plates of good wheels.

To find a defective wheel at the earliest possible time prior to failure smaller and smaller cracks must be found. The problem with crack detection methods is that the smaller the cracks, the larger the cost of testing. In the limit, cracks smaller than the wavelength may altogether go undetected. This may not be significant in the case of one small internal crack, but would be of concern if there were a matrix of closed or internal cracks in a wheel. Such a minute crack system may go undetected by eddy current or ultrasonic means.

1.3 Rationale, Test Objectives

In an old test method (still in use in Europe) when the train pulled into the depot the brakeman walked along the train and tapped each wheel with a 15 pound hammer. He would listen to the ring of each wheel to find the defective ones. This old method relied on the trained ear of the brakeman to find defective wheels.

If this method could be automated with electronic instrumentation it would offer a superior alternative to current visual and ultrasonic crack detection methods.

For this thesis an investigation was made of the low frequency response (20 Hz-20 kHz) of 1/4 scale wheels. A vibrating system resonates at distinct resonant frequencies. If that system is altered then the resonant frequencies will change. These changes can be affected by redistributing the mass, or by altering the stiffness. To apply this to nondestructive testing it was necessary to investigate if indeed cracks in wheels do change the stiffness significantly enough, that the changes in resonant frequencies may be consistently detected with reasonably priced and calibrated instrumentation.

Chapter 2

APPARATUS

2.1 Wheels Tested

The wheels used were 1/4 scale models of a 33 inch diameter railroad wheel. The dimensions of the wheel are given in Figure 2.1. All the wheels were made of low carbon steel. Two methods of manufacture were used: in one, the wheels were machined from a low carbon steel plate (approximately .25% carbon content); in the other, a carbon steel casting (approximately .45% carbon content) was made and the tread and hub were machined on a lathe. Three modes of mounting were employed:

1. Unmounted, i.e. no axle (see Figure 2.2a).
2. Mounted on a stub axle by shrink fitting (see Figure 2.2b).
3. Two wheels mounted on a full axle by shrink fitting (see Figure 2.3).

Table 2.1 lists all the wheels tested and their properties.

2.2 Test Stands and Test Track

The test stands were constructed to suit the requirements of each of the wheels tested. Wheels 1 through 5 were placed on a wood platform in the anechoic chamber (see Figure 2.4a). An electrodynamic shaker was mounted in a heavy plate bracket, and placed adjacent to the wheel. To elevate the wheels to the axis of the shaker armature, 2x4 wooden shims were used under the wheels. The wood shims were used only for wheels 1 through 5; wheels 6 through 8 were placed as shown in Figure 2.4b. A steel rule was

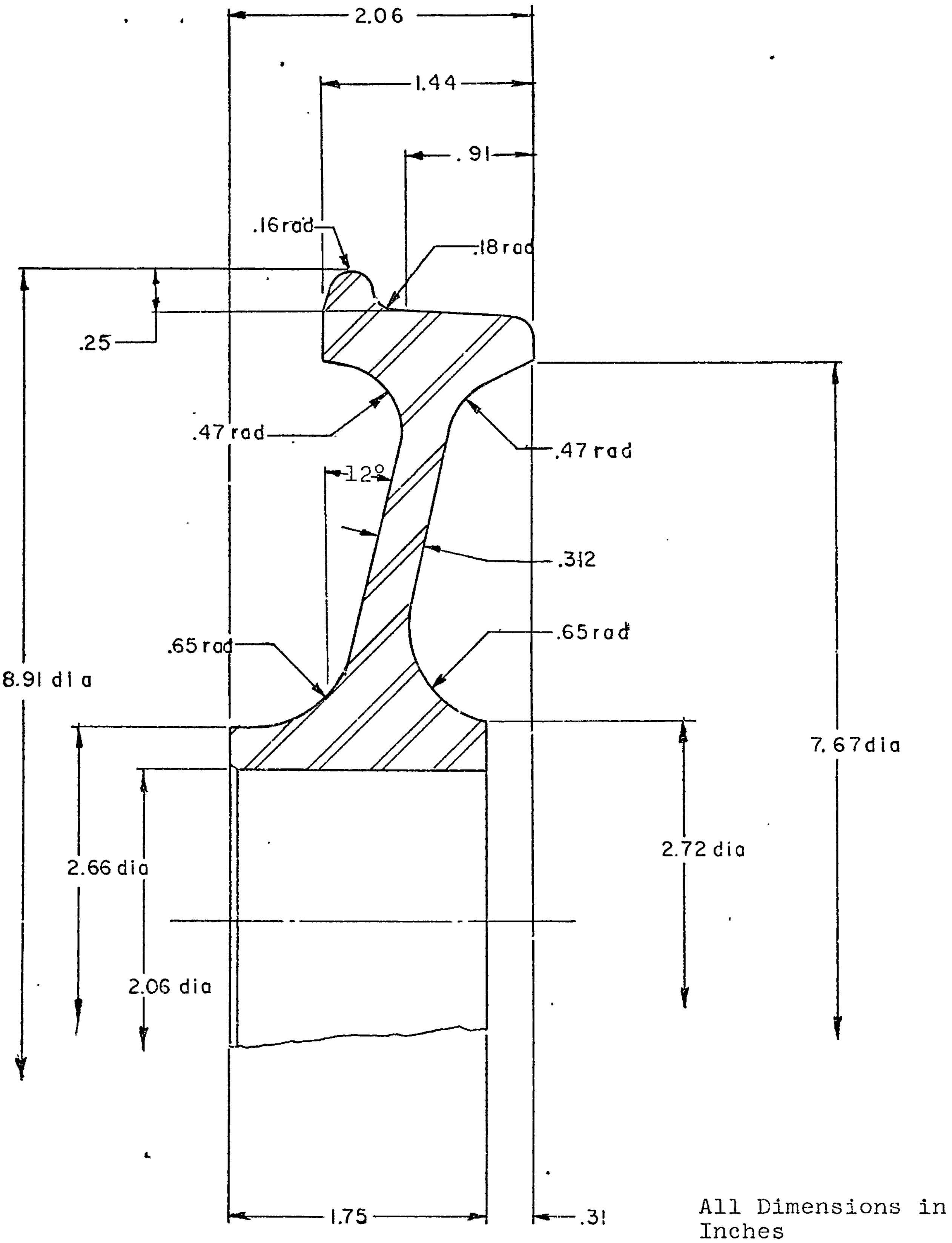

Fig. 2.1 Dimensional Drawing of 1/4 Size Railroad Wheel

Table 2.1 Wheels Tested

Wheel No.	Material	Method of Manufacture	Method of Mounting	Condition of Wheel
1	Carbon Steel	Cast & Machined	No Axle	Good
2	"	"	"	"
3	"	"	"	Crack (see Appendix 1)
4	"	Machined From Plate	"	Good
5	"	"	"	Crack (see Appendix 1)
6	"	"	Stub Axle	Good
7	"	Cast & Machined	"	Crack (see Appendix 1)
8	"	"	"	"
9	"	"	Full Axle	Good
10	"	"	"	"

used to set the wheels the same distance from the shaker for each test run. In these particular tests the shaker armature was in contact with the wheel tread, however there was no bond between shaker and wheel. As a result the shaker would only impart forces to the wheel tread in a radially inward direction toward the axle of the wheel. The purpose of this method was to simulate the real environment, where the wheel tread is similarly acted upon by the railway track and the brake shoes.

Wheels 9 and 10 were mounted on a full axle. In the stationary tests the wheel and axle set were supported by two one-foot long tracks on top of a large concrete block (see Figure 2.5a). The armature of the electrodynamic shaker was attached to the cantilevered stub axle of the wheel with the aid of a No.6 screw and some clamps. The shaker body was suspended above with rubber cords. This method of excitation was chosen to simulate the excitation imparted to the wheel and axle set by the bearings on the railroad car.

For the rolling tests a simple narrow gage track was constructed. 2x4 Timber crossties were nailed to 2x4 timber supports. The 12 pounds/yard ASCE rails were fastened to the crossties with common nails and plate washers. The track assembly was placed on the concrete floor in the vibration laboratory (see Figure 2.6a).

To simulate the bump encountered by a railroad wheel at a rail joint a wood wedge was placed under the rolling wheel as shown in Figure 2.6b.

2.3 Excitation and Measurement Instrumentation

The instrumentation is shown in Figure 2.7.

a. Wheels 1, 2, 3, 4 and 5

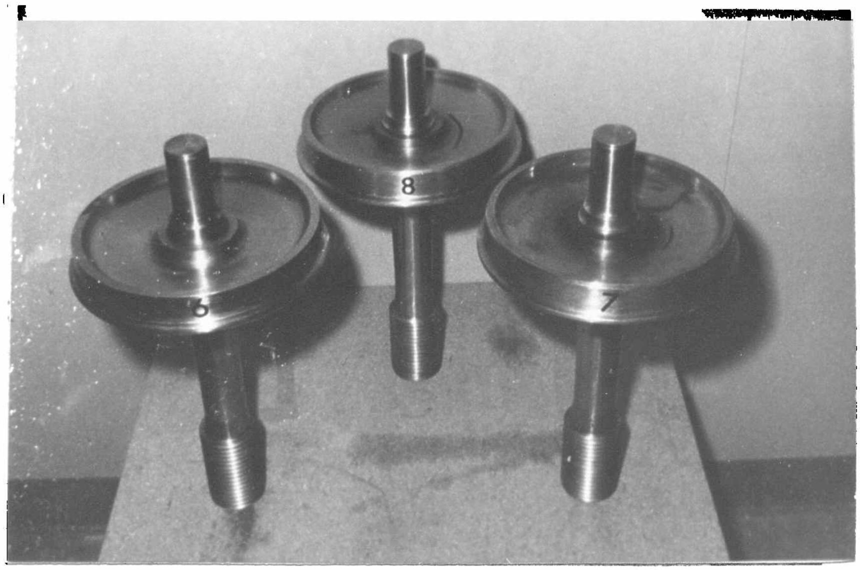

b. Wheels 6, 7 and 8

Fig. 2.2 Model Wheels Tested

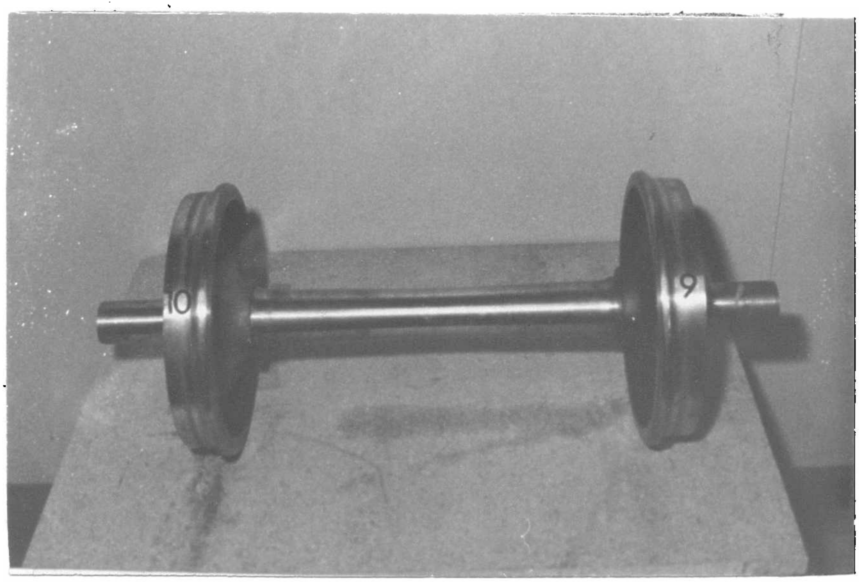

Fig. 2.3 Wheels 9 and 10 Mounted on Full Axle

a. Unmounted Wheels

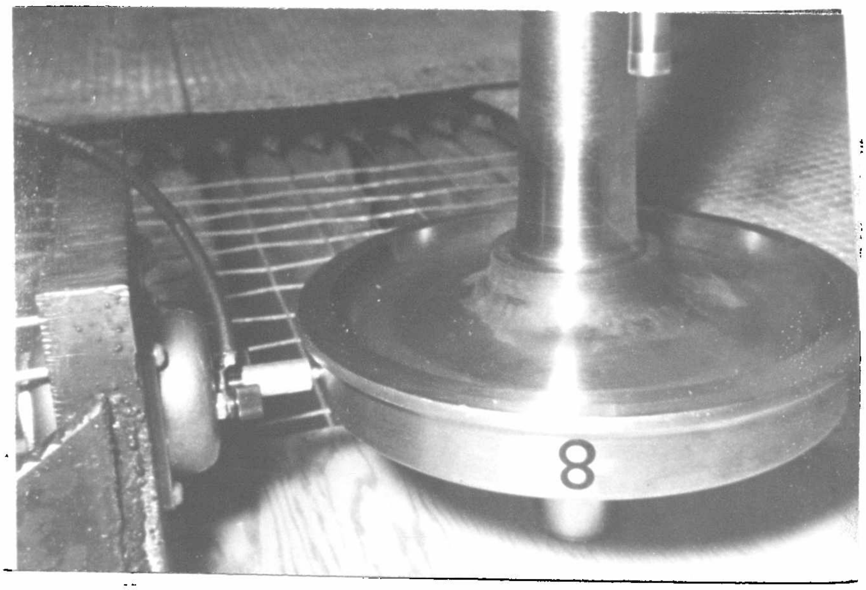

b. Wheels with Stub Axles

Fig. 2.4 Test Stands in Anechoic Chamber

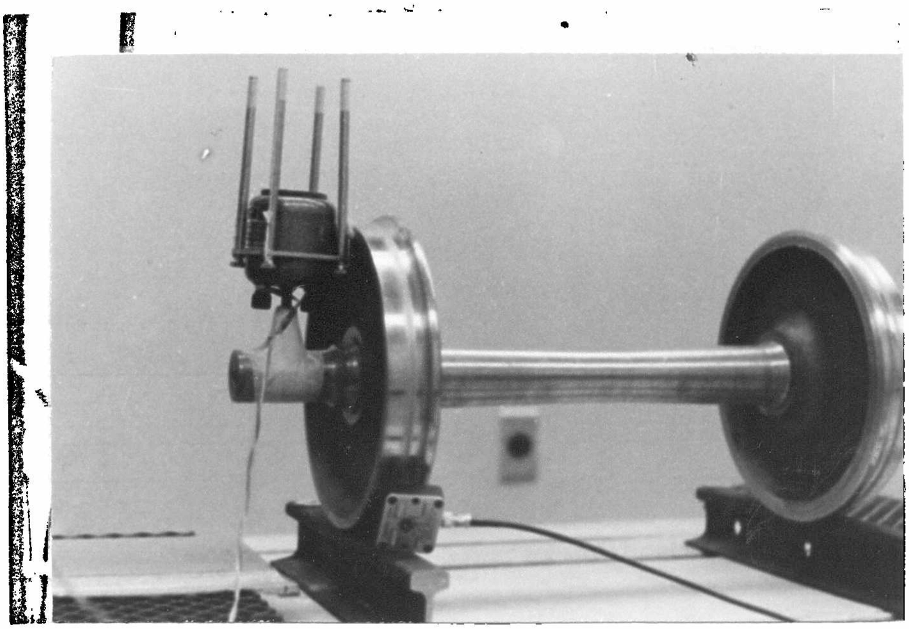

a. Wheels 9 and 10 with Shaker

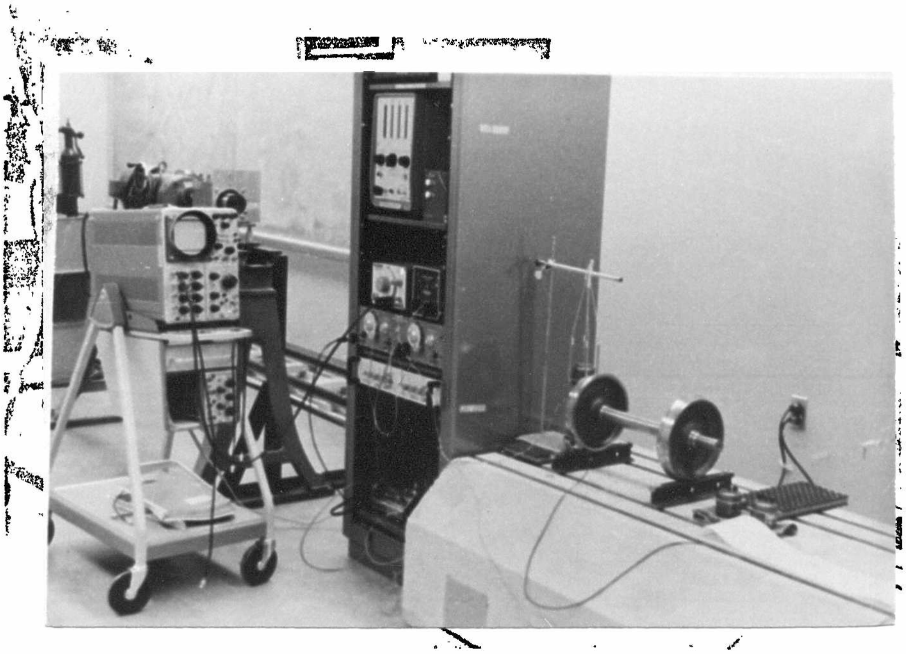

b. Seismic Mass and Instrumentation Arrangement.

Fig. 2.5 Test Stand in Vibration Laboratory

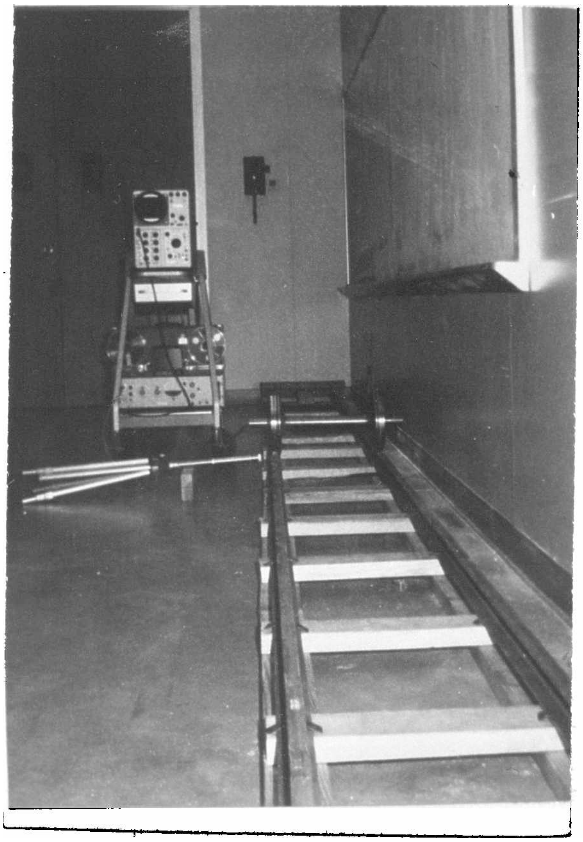

a. View of Track

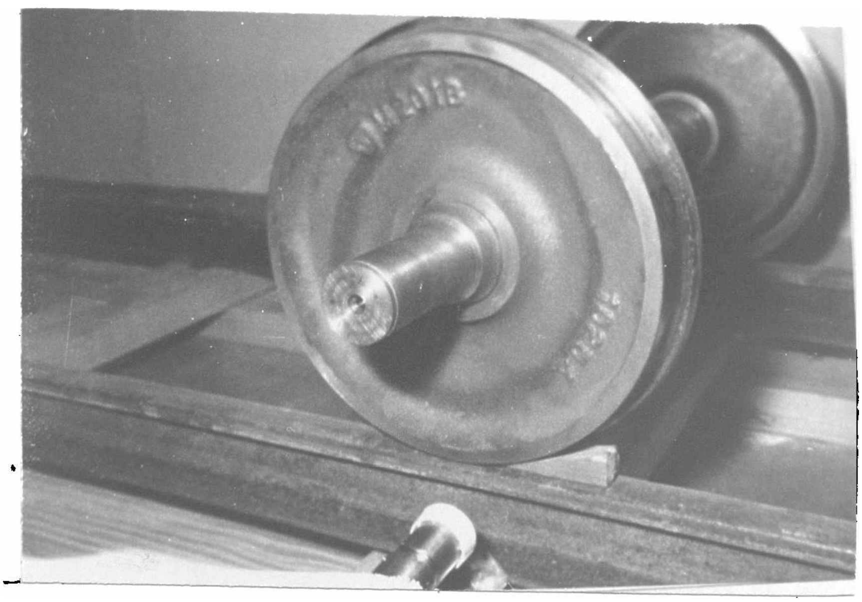

b. View of Wedge on Track

Fig. 2.6 Test Track

The following parameters were monitored in the experiment:

a. airborne sound

b. displacement

c. acceleration

The electronic instrumentation was used for the following purpose:

a. driving the electrodynamic shaker, and

b. the analysis of the amplified signal from the transducer to obtain the frequency spectrum.

The instruments were assembled to suit the requirements of each individual test setup.

In the preliminary tests wheels 9 and 4 were tested in the vibration laboratory. In these tests the instrumentation was arranged as shown in schematic in Figure 2.8. In the continuous random vibration tests all the wheels were tested in the anechoic chamber, except wheel 9, which was tested in the vibration laboratory. The schematic for these tests is shown in Figure 2.9. For the driving of the shaker all standard equipment was used. However the analysis of the signal was performed on the B&K analyzer. The analyzer will accept an input signal from a variety of transducers, in the 20 Hz to 20 kHz range. The analyzer has the capability to provide a real time 1/3 octave analysis of a continuous or a transient signal. The time constant for the response of the real time analyzer is .2 seconds above 200 Hz and 3.15 seconds maximum below 200 Hz. The 1/3 octave frequency spectrum is displayed on a video screen which shows the linear level in thirty 1/3 octave bands with center frequencies

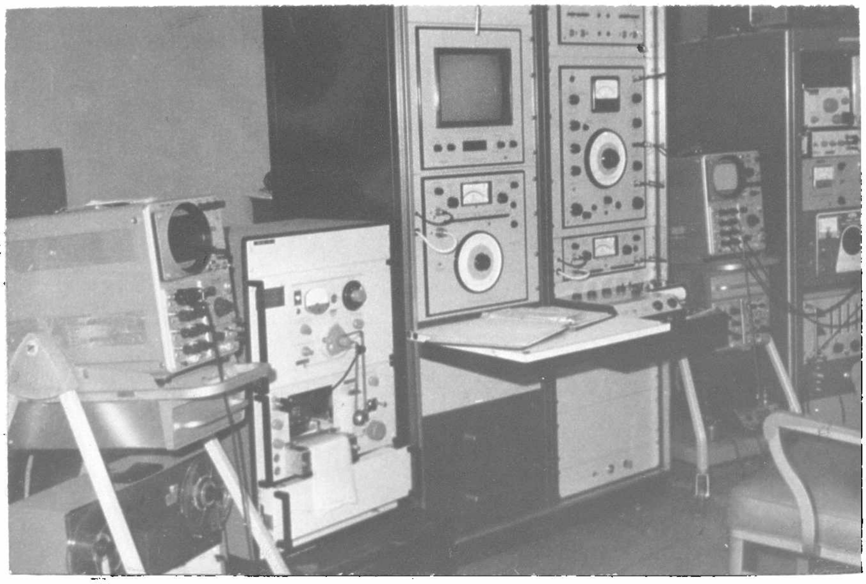

a. Stationary Tests

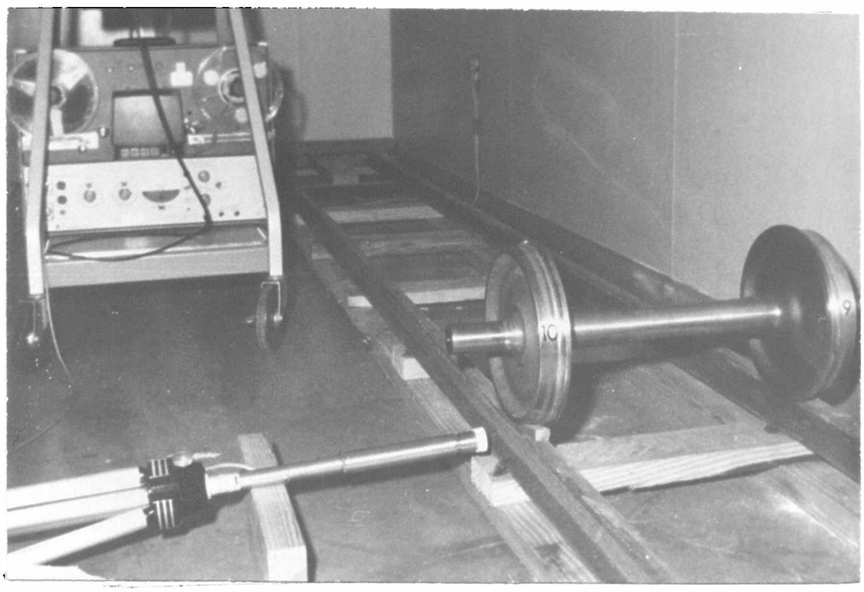

b. Rolling Tests

Fig. 2.7 Instrumentation

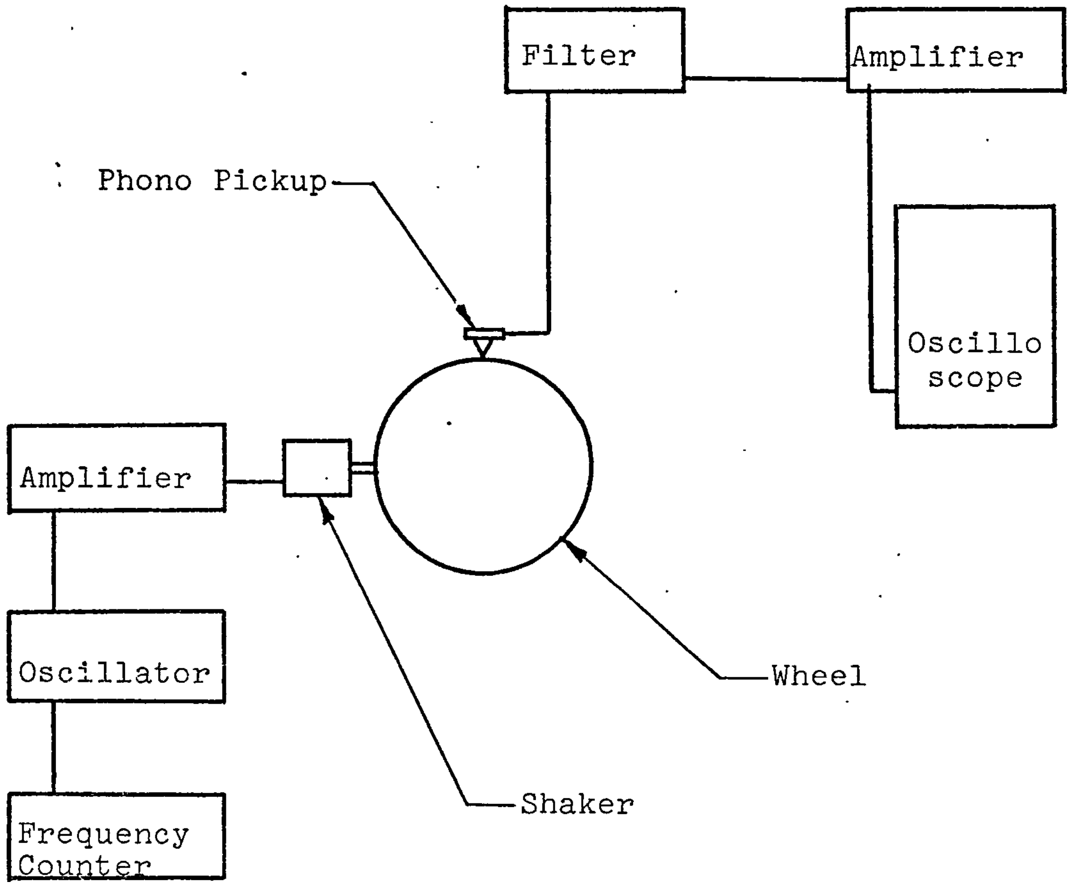

Fig. 2.8 Schematic for Preliminary Investigations

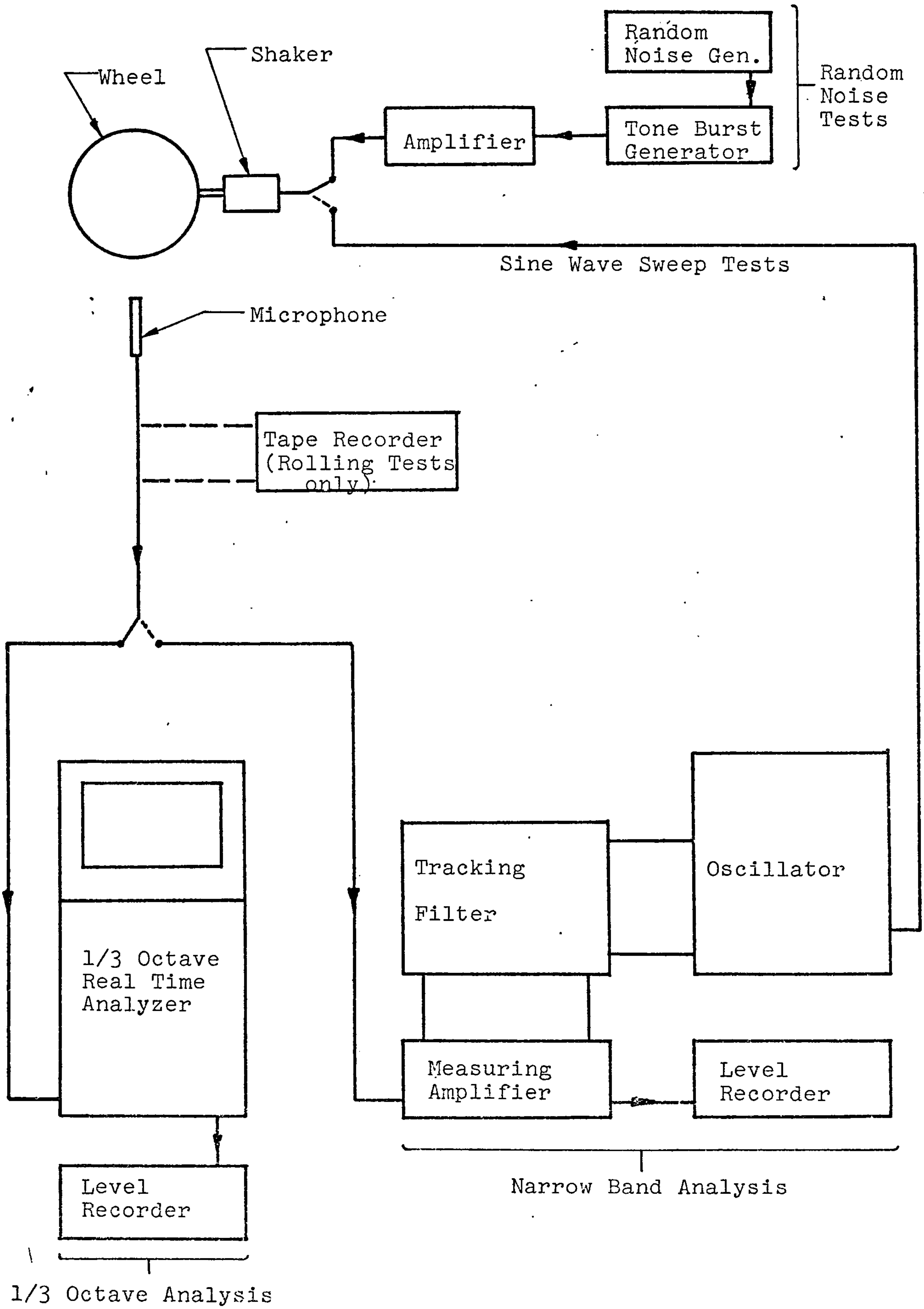

Fig. 2.9 Instrumentation Schematic

ranging from 25 Hz to 20 kHz. In addition to the 1/3 octave filters, one of the frequency weighting networks A,B,C, or D may be selected, with the option of displaying overall linear level in the range from 22.4 Hz to 22.0 kHz. The video display at any instant may be stored, and subsequently recorded on chart paper with a level recorder; in this manner a permanent record may be obtained. In ordinary mode the video display will vary as the input signal varies, however in the maximum mode the video display will retain the maximum level reached in each filter and will only change if a new maximum is reached.

The equipment has the added capability of narrow band sweep frequency analysis and sine wave sweep frequency analysis. (In this mode of operation the 1/3 octave real time analyzer is by-passed). The incoming signal is fed into a measuring amplifier and passed through a narrow band tracking filter, which is driven by an oscillator; the oscillator is mechanically driven by a strip chart recorder, thus the frequency band from 20 Hz to 20 kHz is swept. The resulting record is an amplitude versus frequency plot on semilog paper. The narrow band tracking filter also has a $1/\sqrt{B}$ compensation for analysis of random noise, where B is the bandwidth. With the narrow band tracking filter band widths of 3.16, 10, 31.6 and 100 Hz were available.

Chapter 3

EXPERIMENTAL INVESTIGATIONS

The research tests were designed to obtain frequency spectra for wheels excited in a variety of ways. Simulated cracks were machined by electrodischarge machining in the plate of wheels 3, 7 and 8 (see Appendix 1). The frequency spectra of all wheels were recorded.

3.1 Preliminary Investigations

The initial tests were performed without the use of the B&K analyzer, to obtain resonant frequencies. Wheels 9 and 4 were tested as shown in Figures 2.5 and 2.6. The electrodynamic shaker imparted a force to the wheel that varied in a pure sinusoidal manner, and the resonant frequencies were obtained by manually sweeping the frequency band on the oscillator. The frequency was varied from 20 Hz to 20 kHz. The response of the wheel was monitored with a phonograph pickup, and the amplified signal from the pickup was displayed on a oscilloscope. At each resonant frequency the signal peaked at a much higher level than at non-resonant frequencies. Thus the resonant frequencies were obtained by reading the numerical value of the frequency on the counter when a maximum signal level was displayed on the oscilloscope screen. It must be noted that this manner of testing was slow and time consuming, and the repeatability of the test was not very good.

3.2 Continuous Random Vibration Tests

The continuous random vibration tests were conducted to provide frequency spectra for all the test wheels. The wheels were tested with the test setups described in Section 2.2. In these tests the electrodynamic shaker imparted a random force input to the wheels with components over the frequency range of 20 Hz to 50 kHz. This method of excitation was choosen for two reasons: firstly, it was expected that in actual service a railroad wheel will receive a variety of exciting forces that vary in a random manner; secondly, the wide band random excitation provided the most readily reproducible results. The response of the wheels was monitored with microphones and accelerometers. The response signals were analysed with the B&K frequency analyzer, and the resulting frequency spectra were recorded.

3.3 Continuous Sine Wave Tests

The continuous sine wave tests duplicated the experiment that is described in Section 3.1. However the B&K analyzer was employed to provide a continuously varying sine wave sweep signal to the electrodynamic shaker. This signal changed at a constant rate, rather than at an irregular rate provided by manually turning the controls on the oscillator as done in the preliminary tests. The sweep rate of the analyzer was varied to investigate its effect on the results.

3.4 Impact Tests

In these tests the electrodynamic shaker was operated as a tapper. A random noise signal to the shaker was periodically interrupted using a tone burst generator. The resulting random noise pulses caused a small metal hammer attached to the armature of the shaker to strike the wheel. The pulse duration and pulse separation was varied from test to test to investigate its effect on the frequency spectra of the wheels. The response of the wheels was analysed with the B&K analyzer. In this case not only were frequency spectra generated, but also the decay of these spectra with time could be, and was, investigated.

3.5 Rolling Noise Tests

Rolling noise tests were made on a 30 ft. length of track with wheels 9 and 10 which were mounted on a full axle. The wheels were rolled down the track and the rolling contact noise was recorded on a tape recorder. Tests were made also by rolling the wheel over a wooden wedge. This was an attempt to duplicate the impact that a full size railroad wheel receives at a rail joint.

When a full size wheel rolls in a very sharp curve or when it passes through a speed retarder, as used in some railroad yards, intense sound output is generated. This method of excitation was duplicated by rolling the wheel and axle set at an offset angle on the tracks. The flange then contacted the track and the wheel emitted a high pitched scream.

3.6 Shaker Resonance Test

Load tests were performed to obtain the resonant frequencies for the shaker. The tests were conducted in the anechoic chamber; the response of the shaker was analysed with the B&K analyzer. The shaker was again operated with a 50 kHz bandwidth random noise input signal.

Chapter 4

RESULTS

4.1 Preliminary Investigations

The initial tests (see Section 3.1) provided resonant frequencies for wheels 9 and 4. These experimentally obtained resonant frequencies are tabulated in Table 4.1, together with the theoretical resonant frequencies and the experimental resonant frequencies for the shaker. It should be noted that these initial tests were performed for wheels 9 and 4 only and that neither of these wheels had a simulated crack in it. Thus no comparisons could be made between good and cracked wheels.

4.2 Continuous Random Vibration Tests

The narrow band frequency spectra (recorded with a 3.16 Hz bandwidth tracking filter) for wheels 1 through 8 are shown in Figures 4.1 through 4.4. Comparative tests were run for wheels 1, 2 and 3. The frequency spectra for these wheels were plotted on the same chart paper. Graphs were plotted for spectra obtained with 3.16, 10, 31.6, 100 Hz and 1/3 octave bandwidth filters (see Figures 4.5,4.6 and 4.7). Wheels 1 and 2 were cast iron wheels without a simulated crack, and without a stub axle. Wheel 3 was cast iron with a simulated crack and no stub axle. All the graphs show differences between wheels 1, 2 and 3. It must be noted that the frequency spectra of wheel 3 consistently differed from wheels 1 and 2.

Table 4.1 Resonant Frequencies Obtained in Preliminary Tests, Theoretical Resonant Frequencies and Shaker Resonant Frequencies

Wheel 9 Tests		Wheel 4 Tests	Estimated Resonances for Wheel	Shaker Resonances
12	8595	20	780	47
20	8712	123	1450	97
135	8949	133	1640	300
203	9197	145	1700	990
218	9474	160	2620	1200
260	9672	177	4700	2050
279	.	186	12100	2500
292	.	199	24200	2800
367	.	213		3100
468	.	400		4600
510		528		6100
585		1381		
681		1493		
717		1592		
878		2983		
1017		4176		
1146		5863		
1392		6894		
1603		7380		
1724		8142		
1776		8196		
1870		9351		
2030		10437		
2207				
2360				
2432				
2511				
2584				
2829				
3186				
3260				
3397				
3747				
4042				
4423				
4590				
5017				
5814				
6110				
7292				
7575				
7846				
8159				

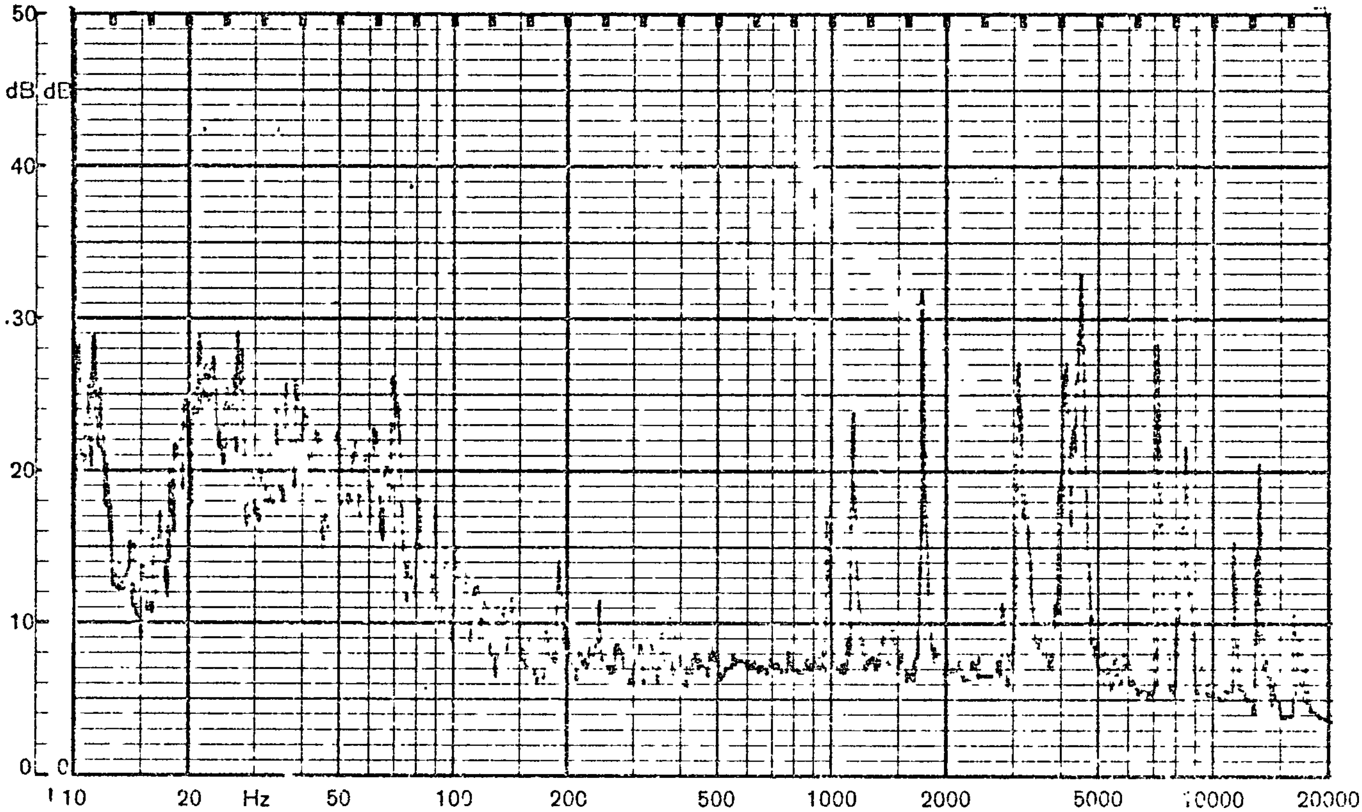

a. Wheel 1

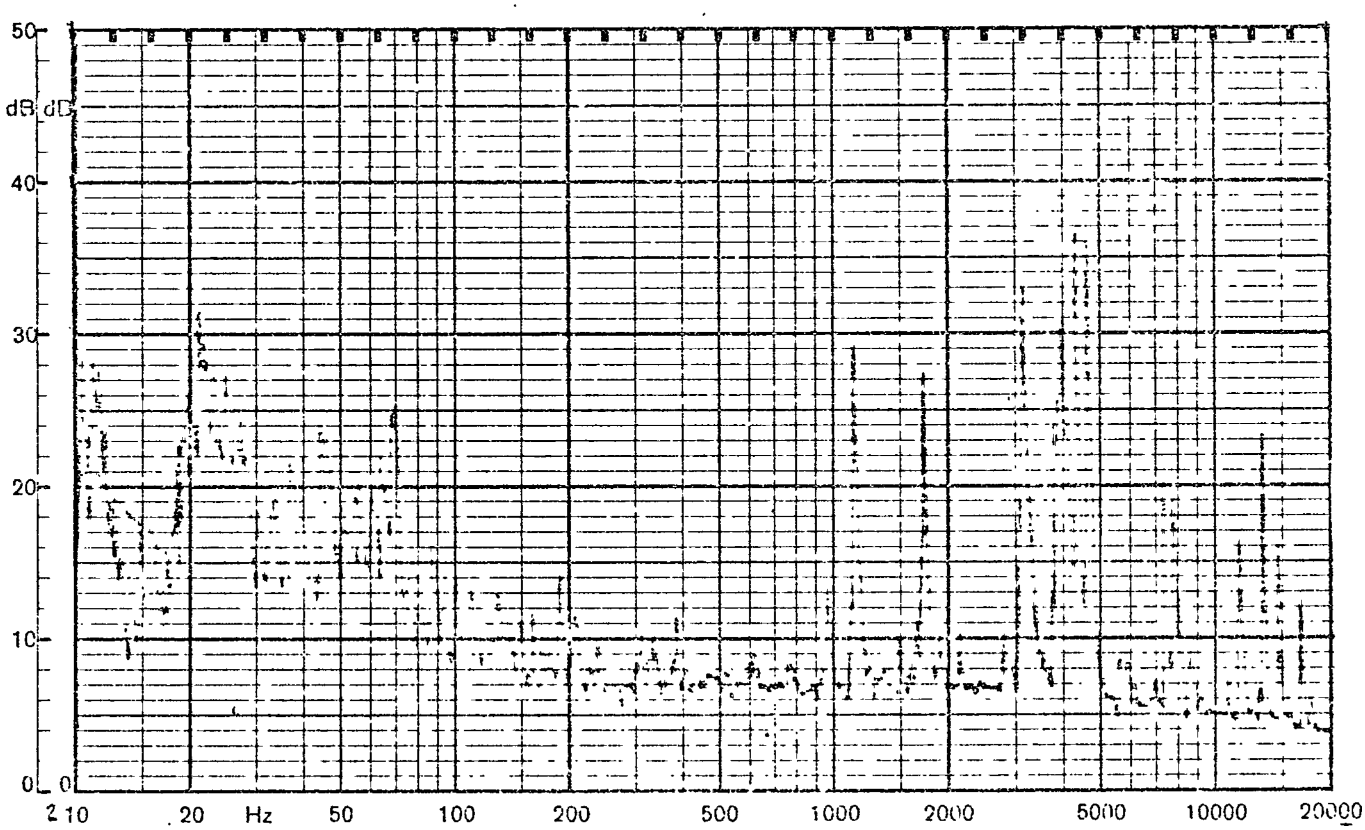

b. Wheel 2

Fig. 4.1 3.16 Hz Bandwidth Frequency Spectra, Random Noise Tests

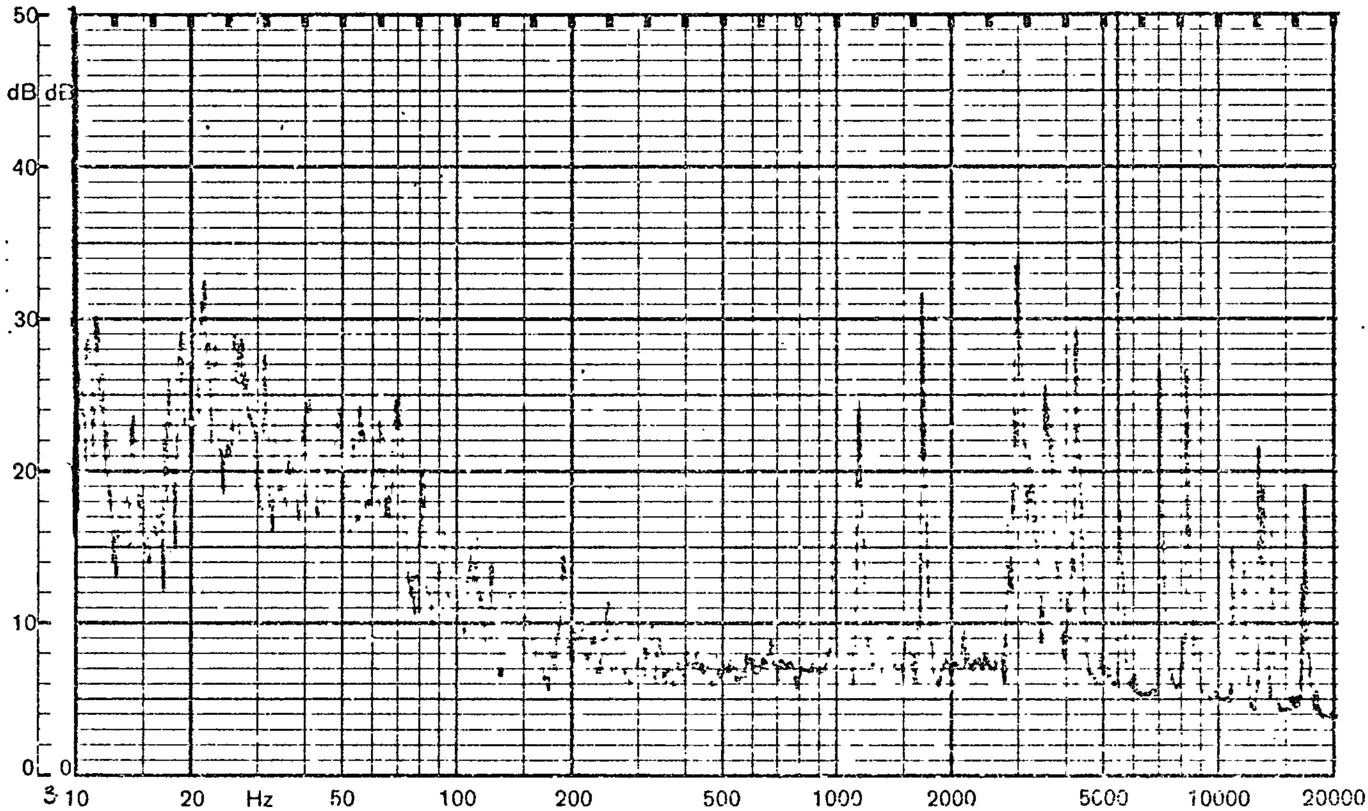

a. Wheel 3

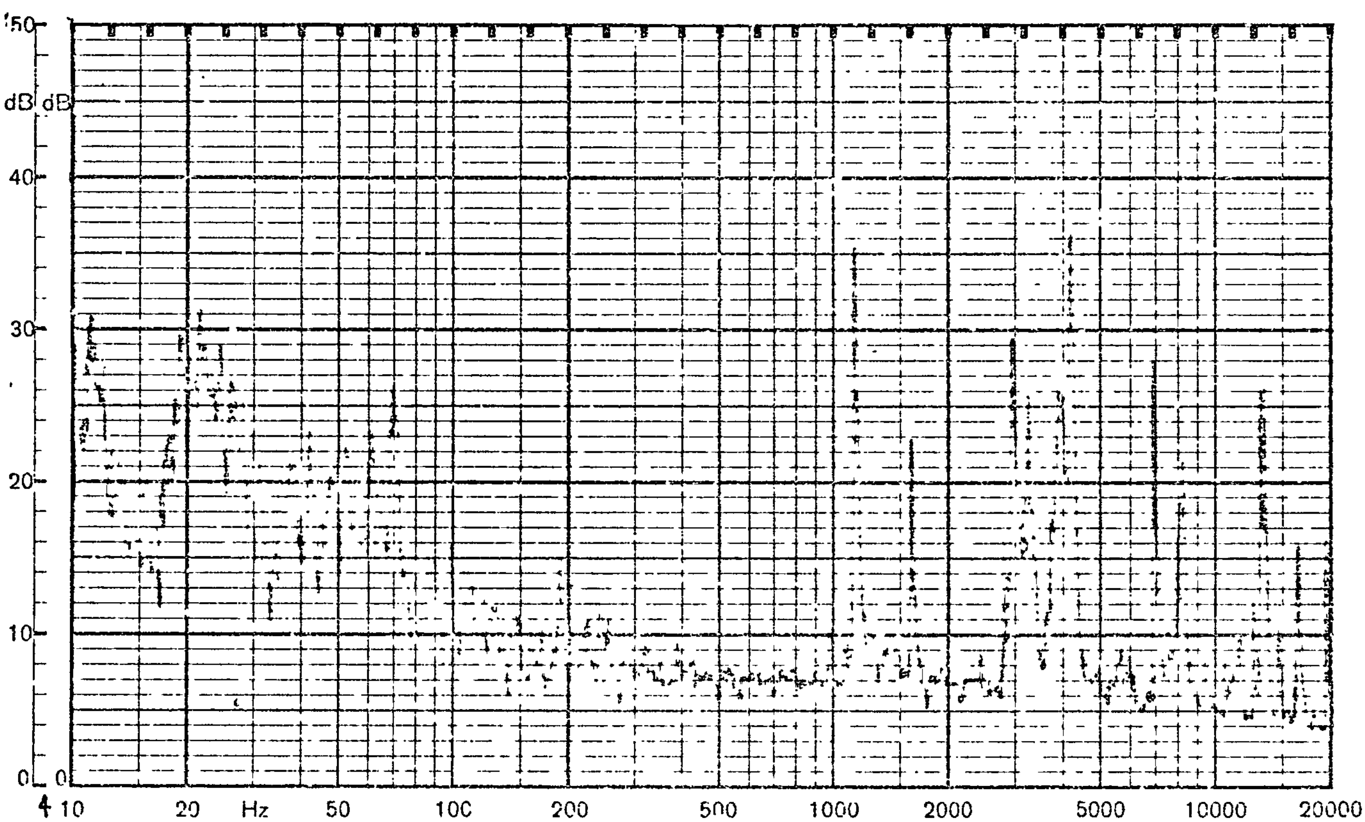

b. Wheel 4

Fig. 4.2 3.16 Hz Bandwidth Frequency Spectra, Random Noise Tests

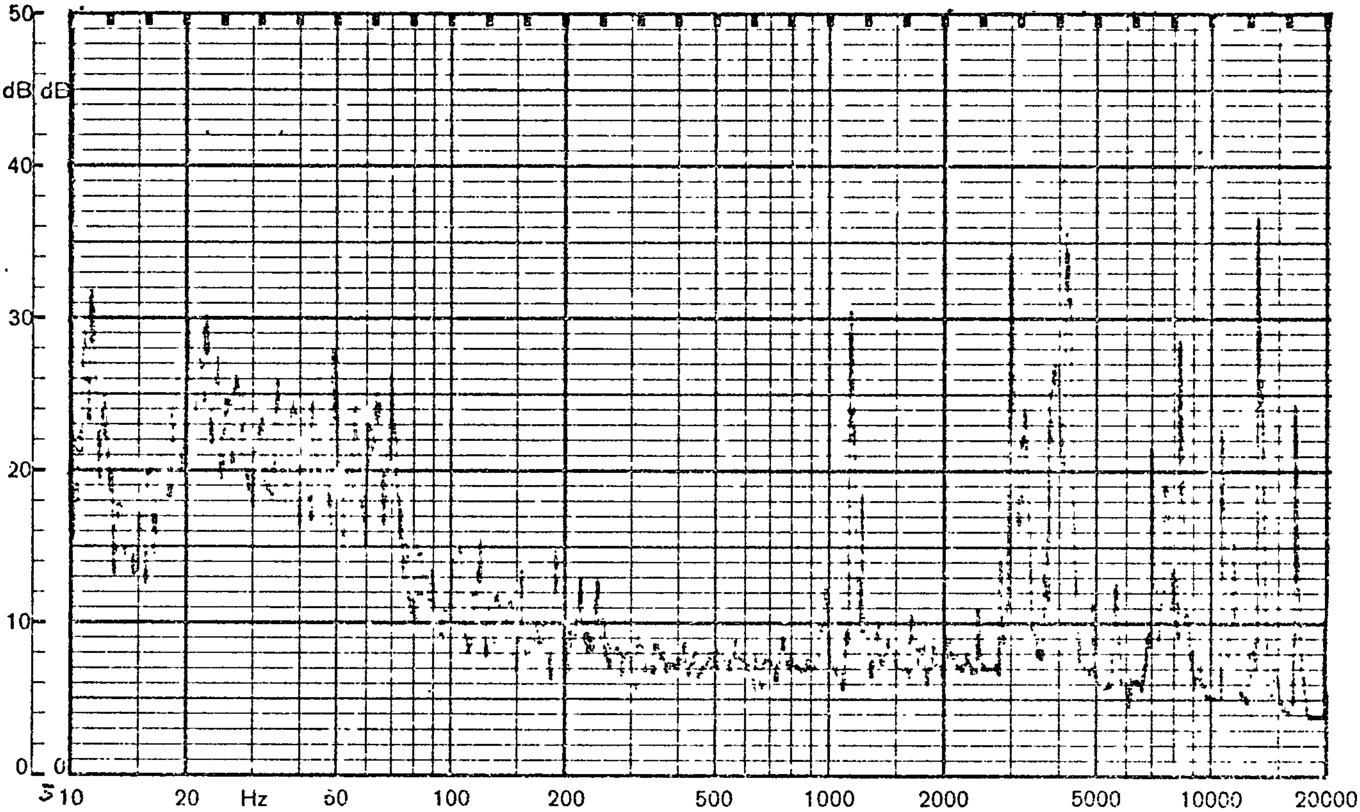

a. Wheel 5

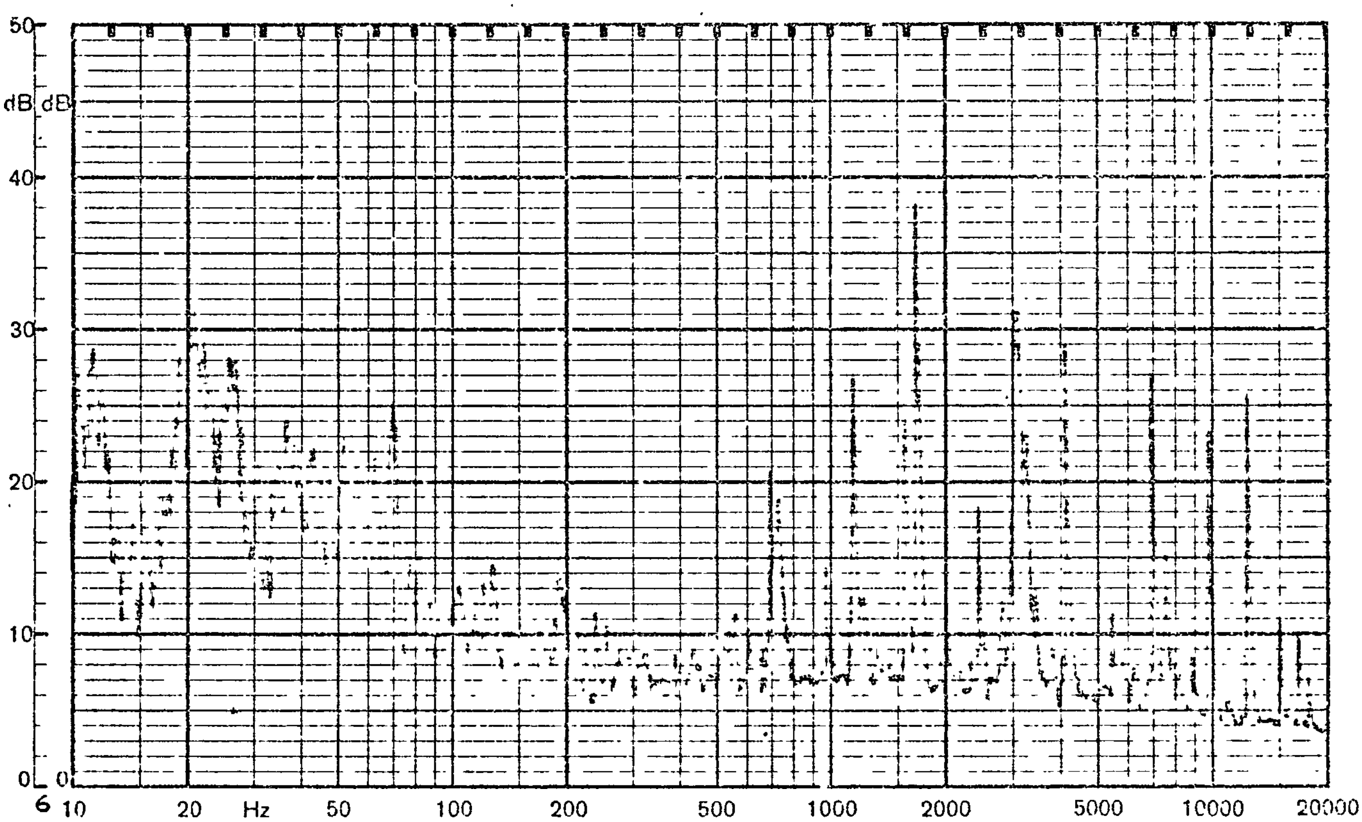

b. Wheel 6

Fig. 4.3 3.16 Hz Bandwidth Frequency Spectra, Random Noise Tests

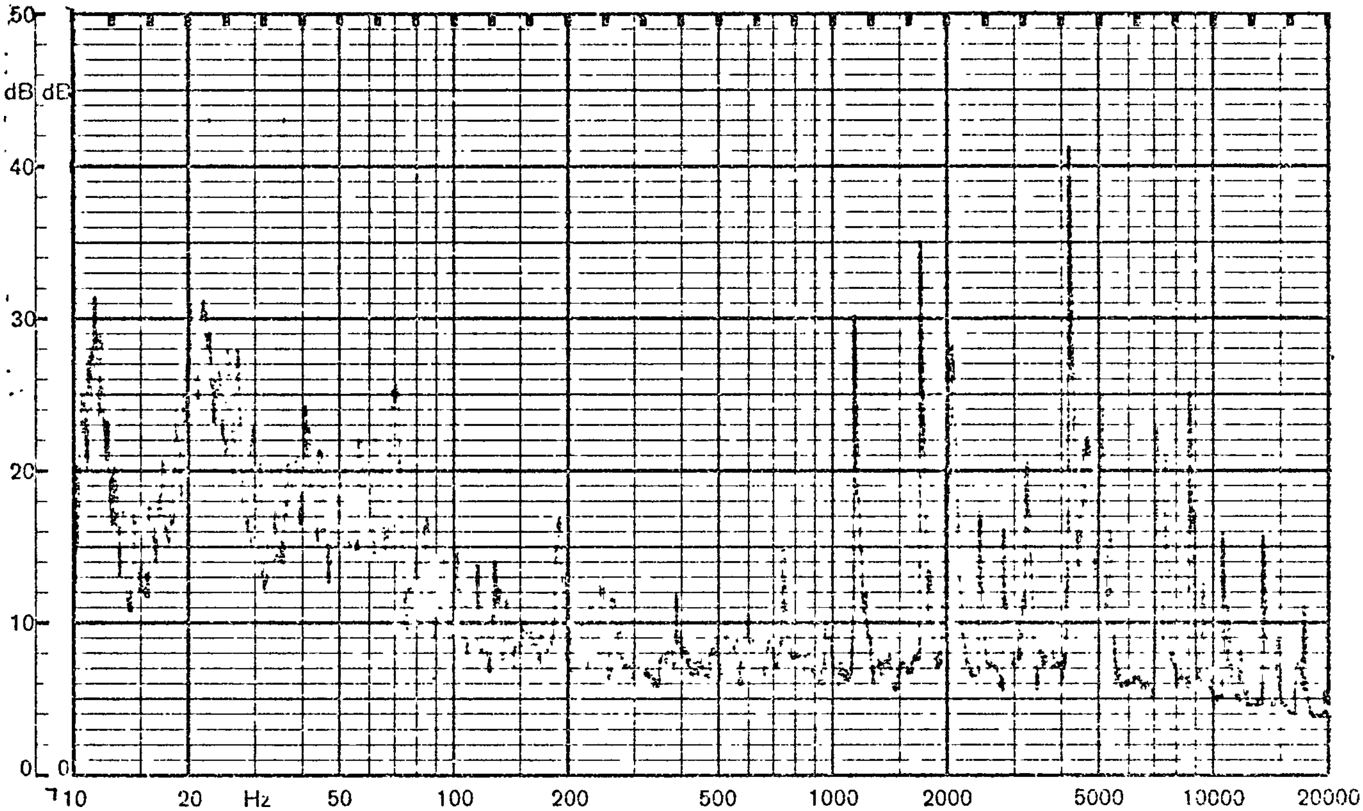

a. Wheel 7

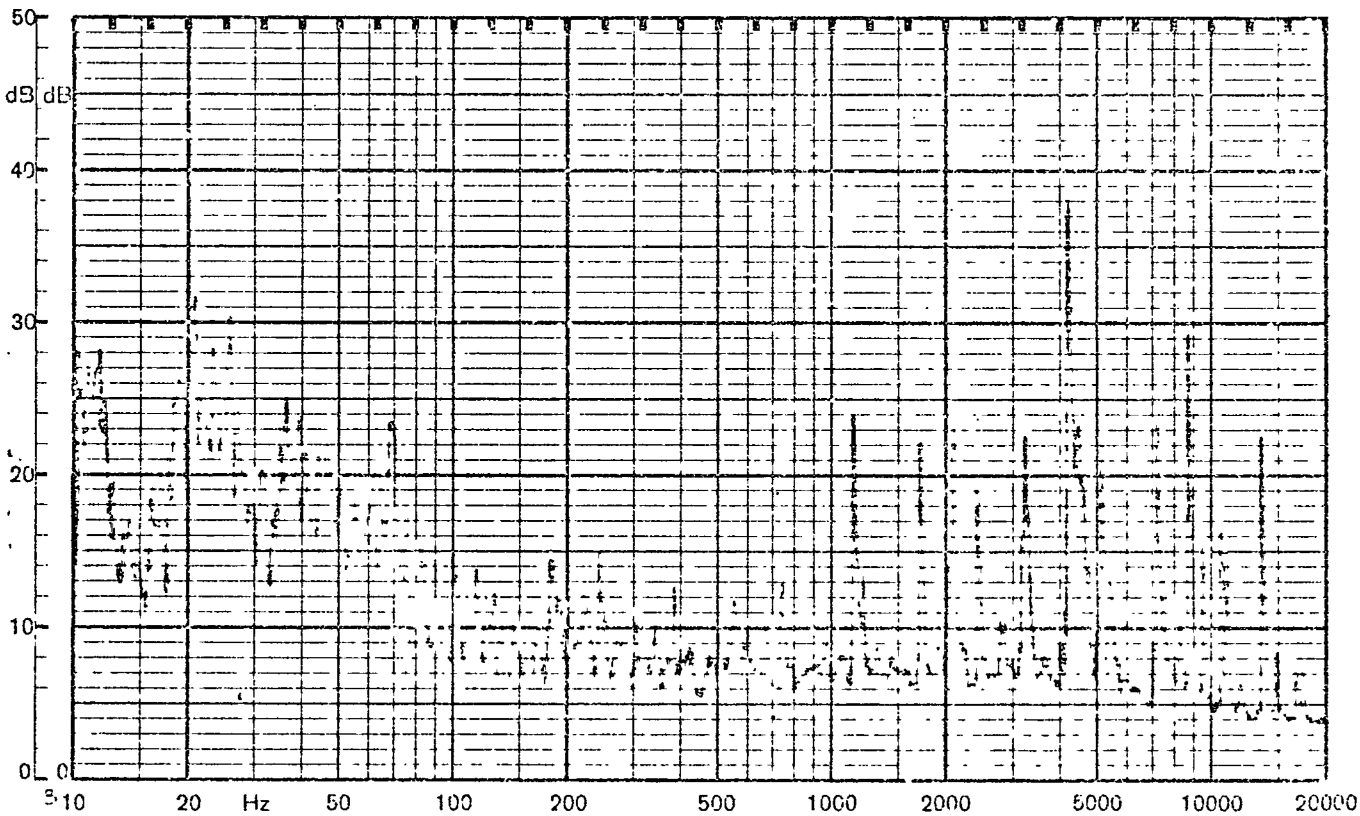

b. Wheel 8

Fig. 4.4 3.16 Hz Bandwidth Frequency Spectra, Random Noise Tests

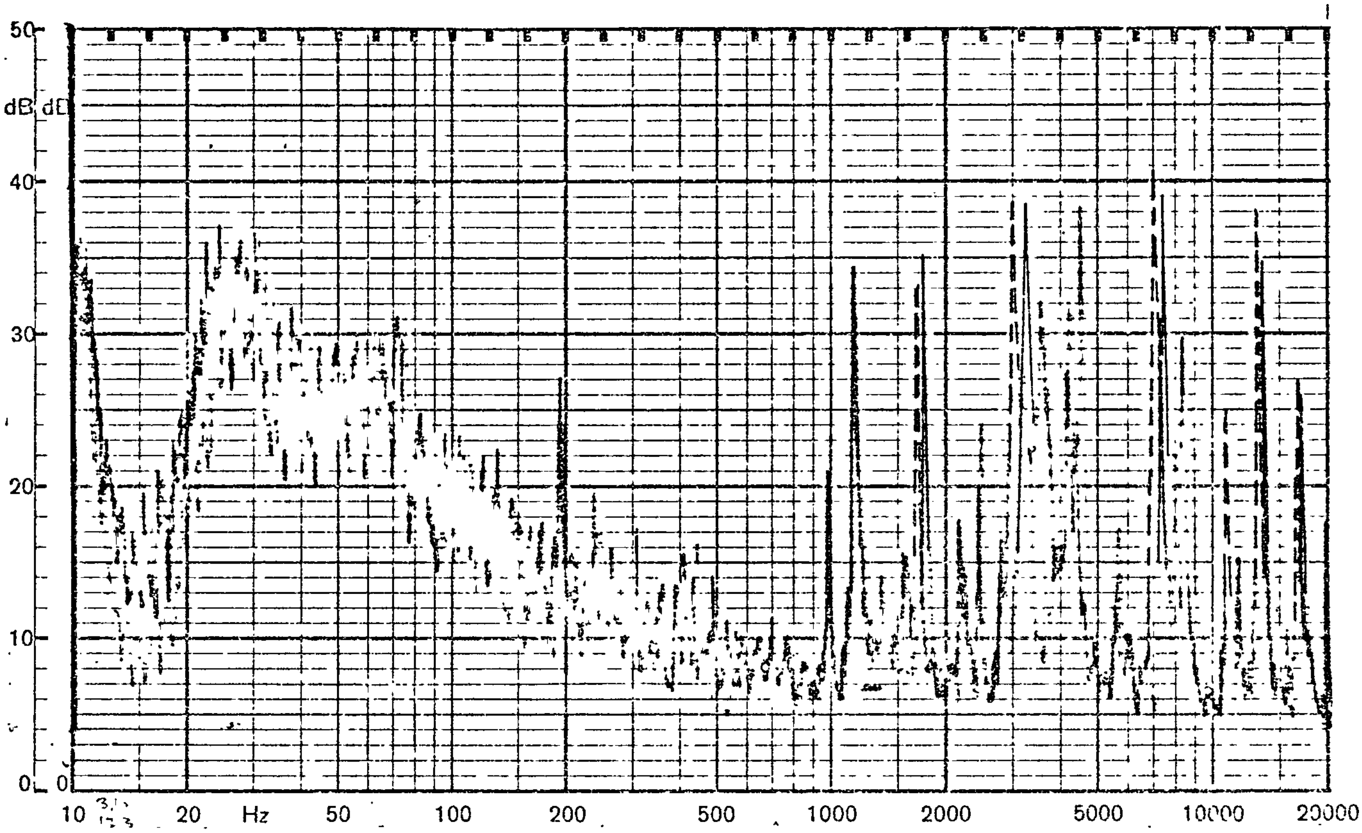

a. 3.16 Hz Bandwidth

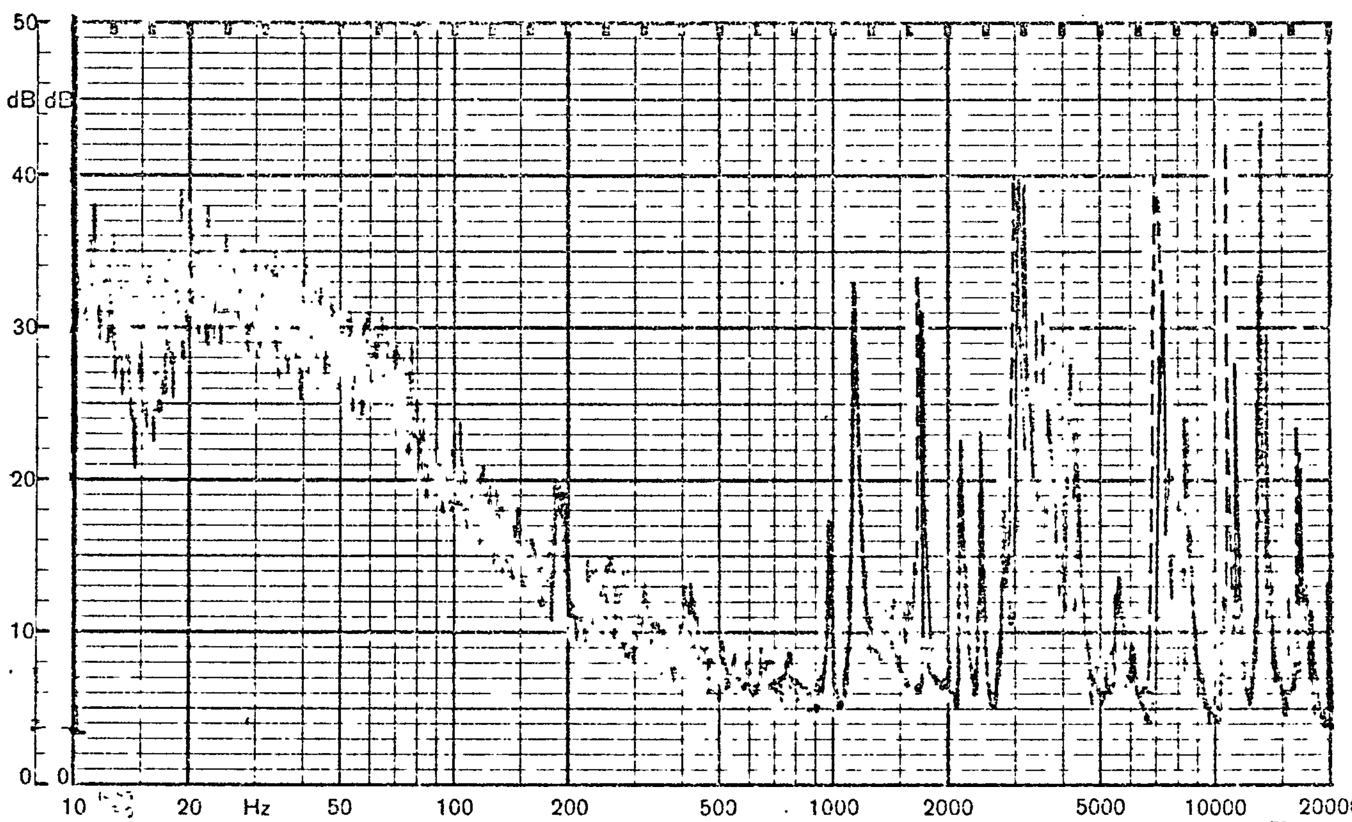

b, 10 Hz Bandwidth

Fig. 4.5 Comparative Graphs for Wheels 1, 2 and 3, Random Noise Tests
(Dashed lines indicate wheel 3 resonances)

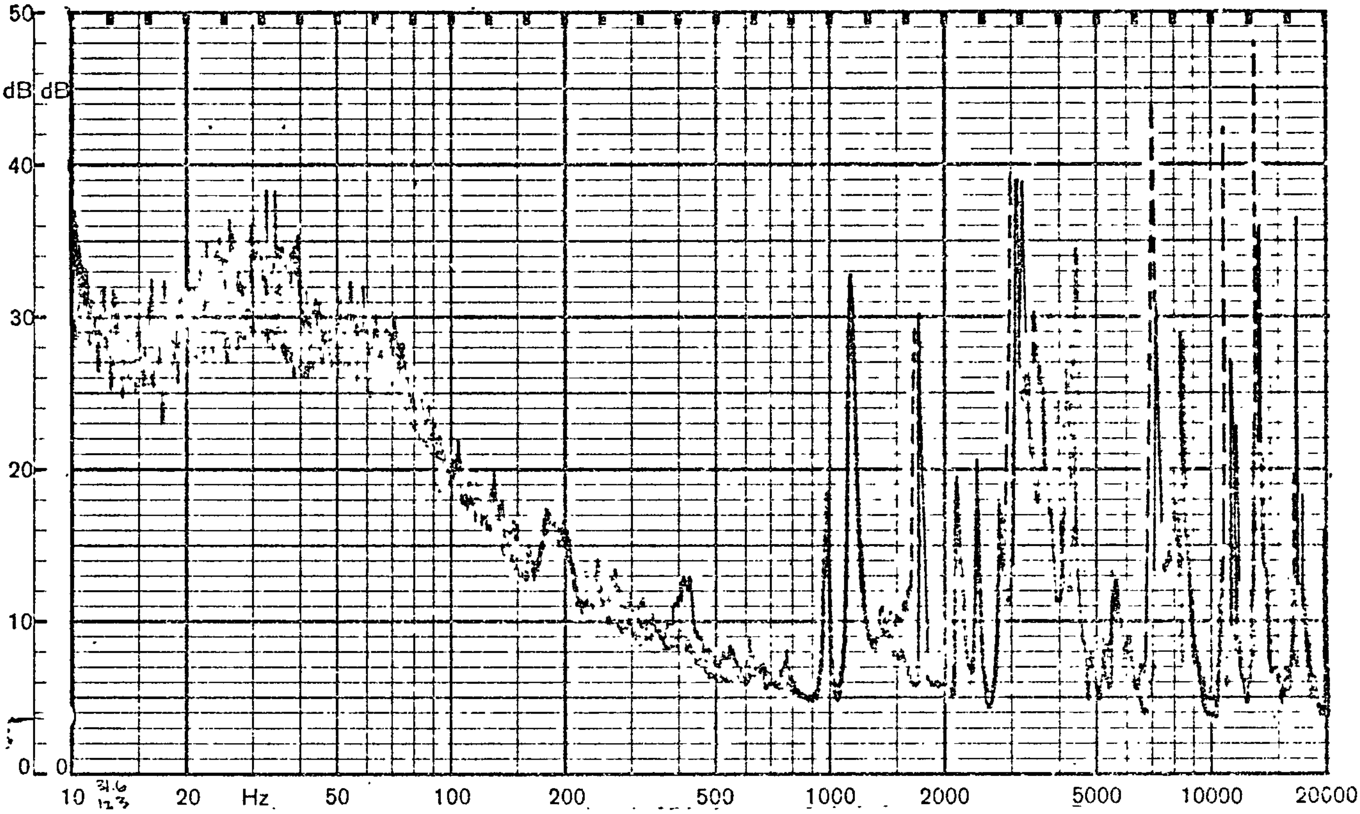

a. 31.6 Hz Bandwidth

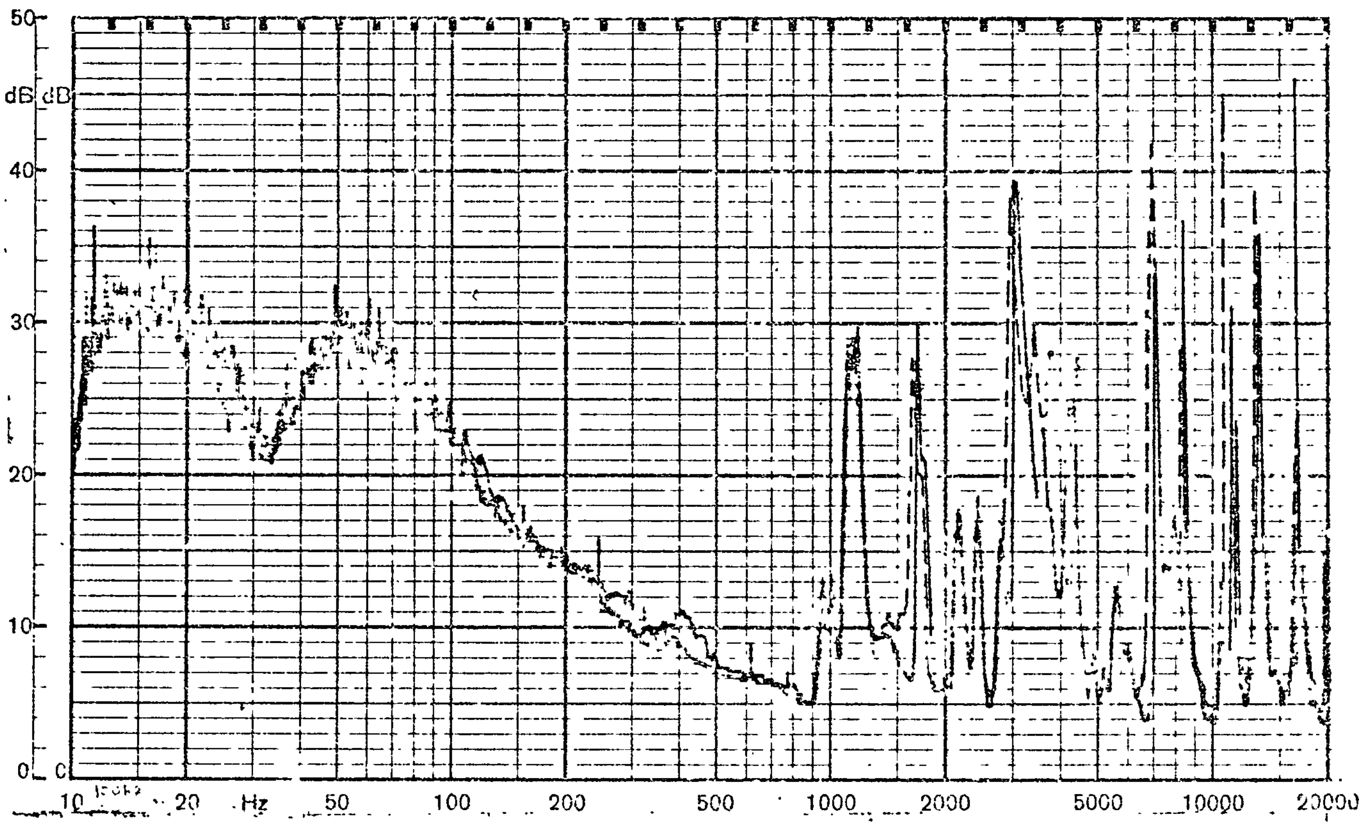

b, 100 Hz Bandwidth

Fig. 4.6 Comparative Graphs for Wheels 1, 2 and 3, Random Noise Tests
(Dashed lines indicate wheel 3 resonances)

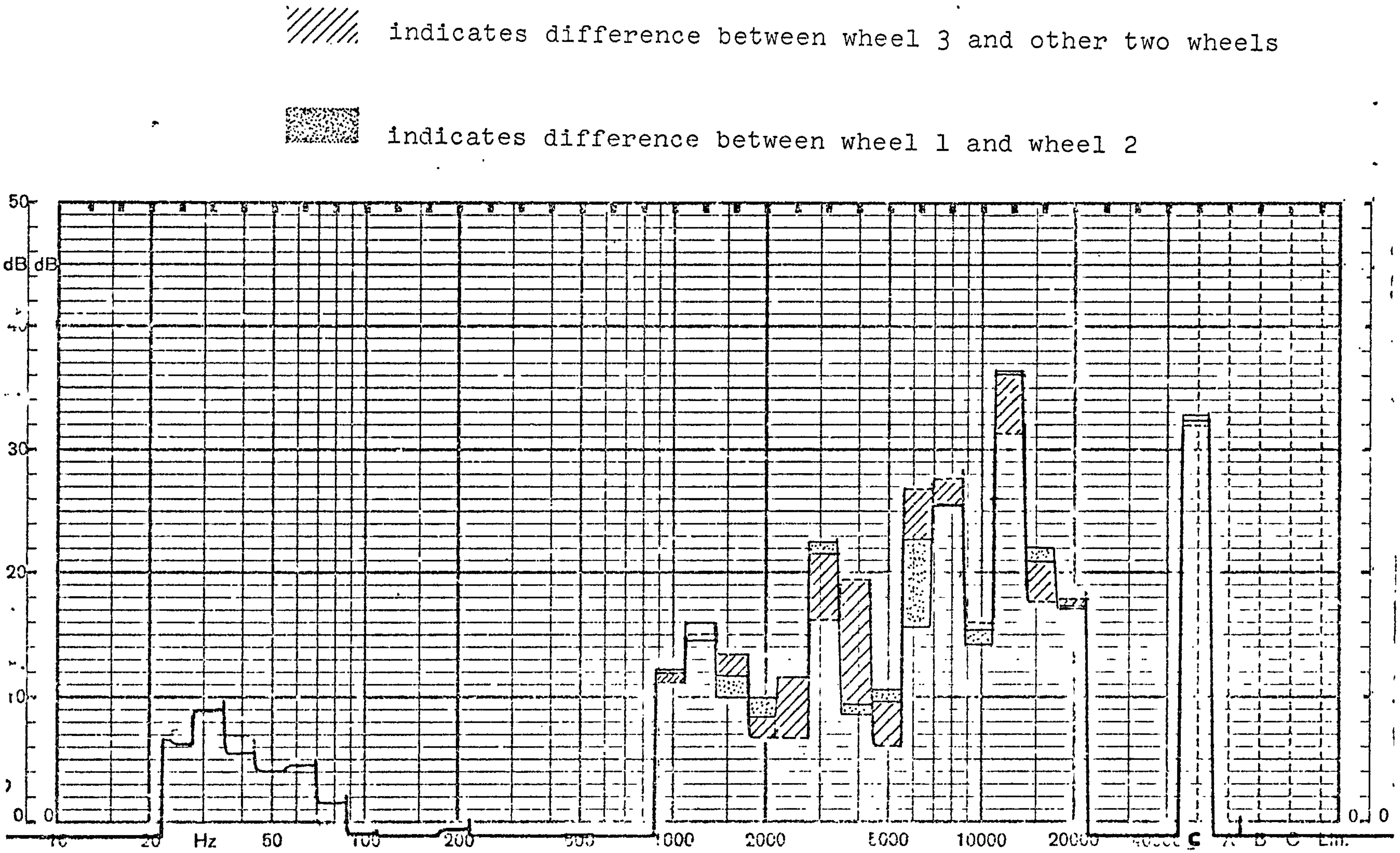

Fig. 4.7 1/3 Octave Comparative Graph for Wheels 1, 2 and 3, Random Noise Tests
(Dashed lines indicate wheel 3 levels)

4.3 Continuous Sine Wave Sweep Tests

Comparative tests were run for wheels 1, 2 and 3. Figure 4.8 shows their frequency spectra obtained with a 3.16 Hz bandwidth tracking filter. Although the spectra are not identical, there are no marked differences between them.

4.4 Impact Tests

Narrow band spectra were not obtained for these tests, since the transient nature of the wheel response did not permit the use of sweep frequency analysis. Instead 1/3 octave frequency spectra were obtained with the B&K real time analyzer, as shown in Figures 4.9 and 4.10a for wheels 1, 2 and 3. Figure 4.10b is a comparative graph for all three of these wheels.

It was observed during the step input tests, that the decay of sound from wheel 3 showed a beating effect, whereas sound from wheels 1 and 2 decayed without this beating. The decay of sound with time was recorded for the three wheels using a 1/3 octave filter with 1.6 kHz center frequency (see Figures 4.11 and 4.12).

4.5 Rolling Noise Tests

Oscillograms were obtained for rolling noise, impact noise when a wheel strikes the track, and scraping noise. These oscillograms are shown in Figures 4.13 and 4.14 . Figure 4.15 shows 1/3 octave frequency spectra for impact noise and scraping noise.

4.6 Shaker Resonance Test

A narrow band frequency spectrum is shown in Figure 4.16 for the test of the shaker with no load. This spectrum was obtained with a 3.16 Hz bandwidth tracking filter.

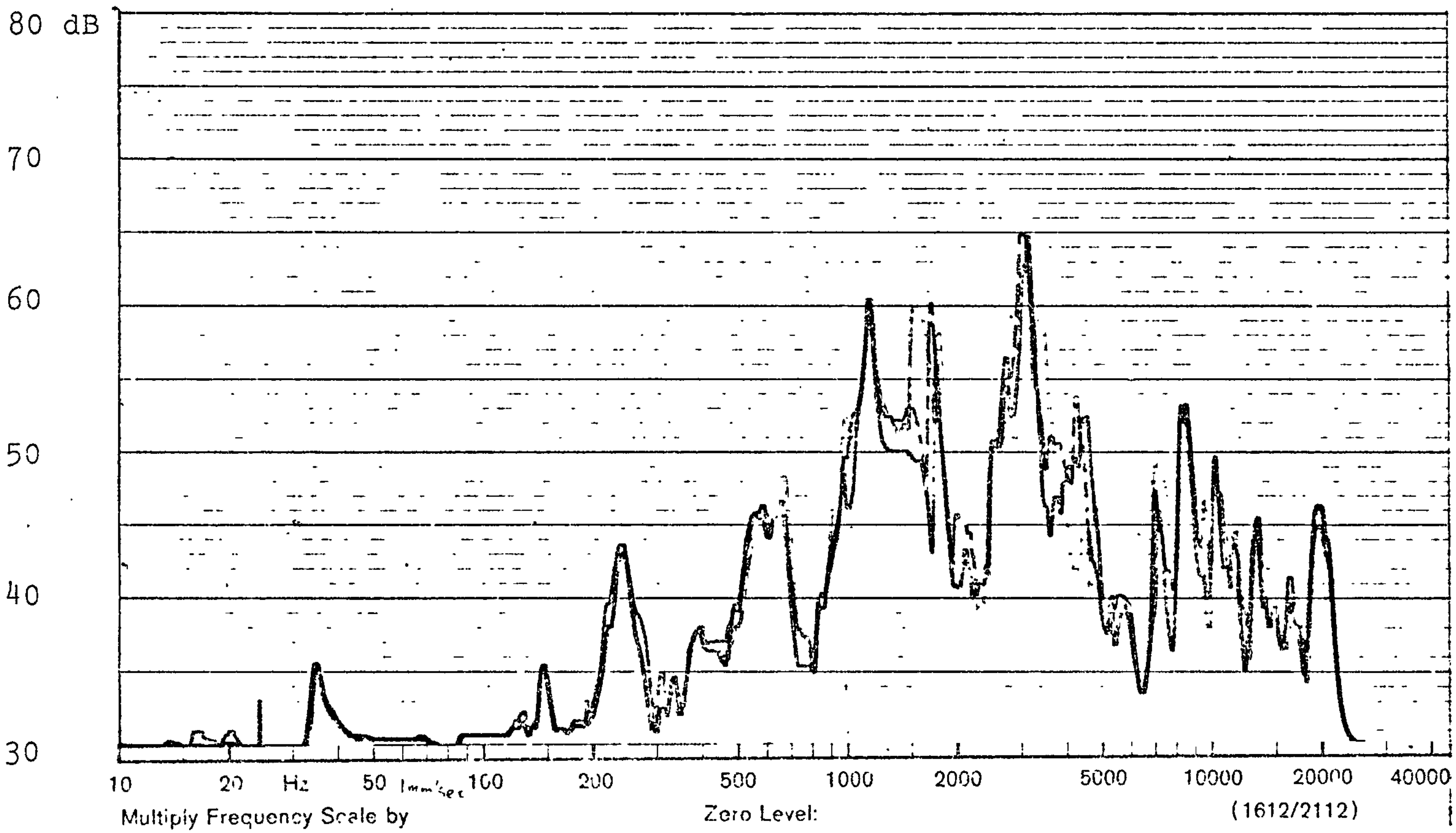

Fig. 4.8 Comparative Graph for Wheels 1, 2 and 3, Sine Wave Sweep Tests

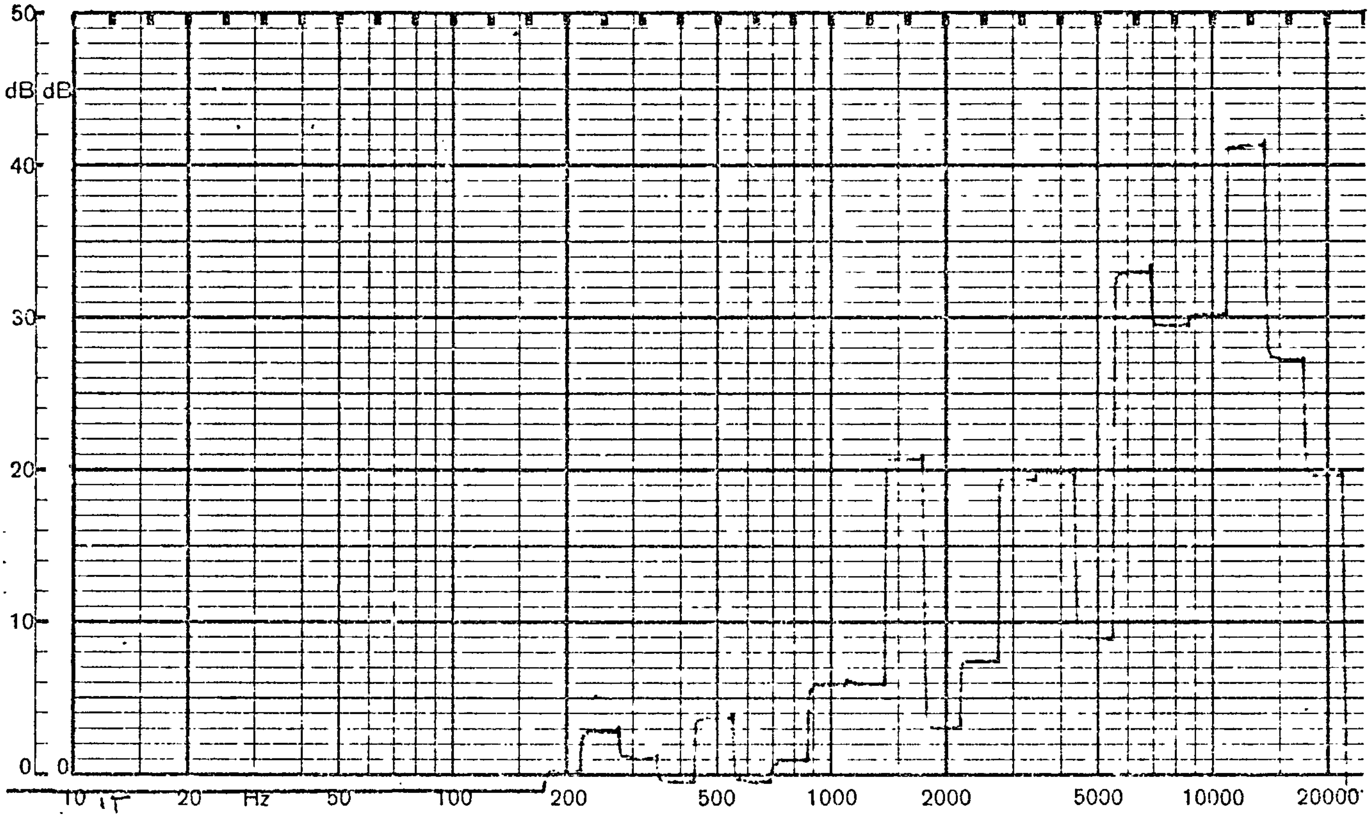

a. Wheel 1

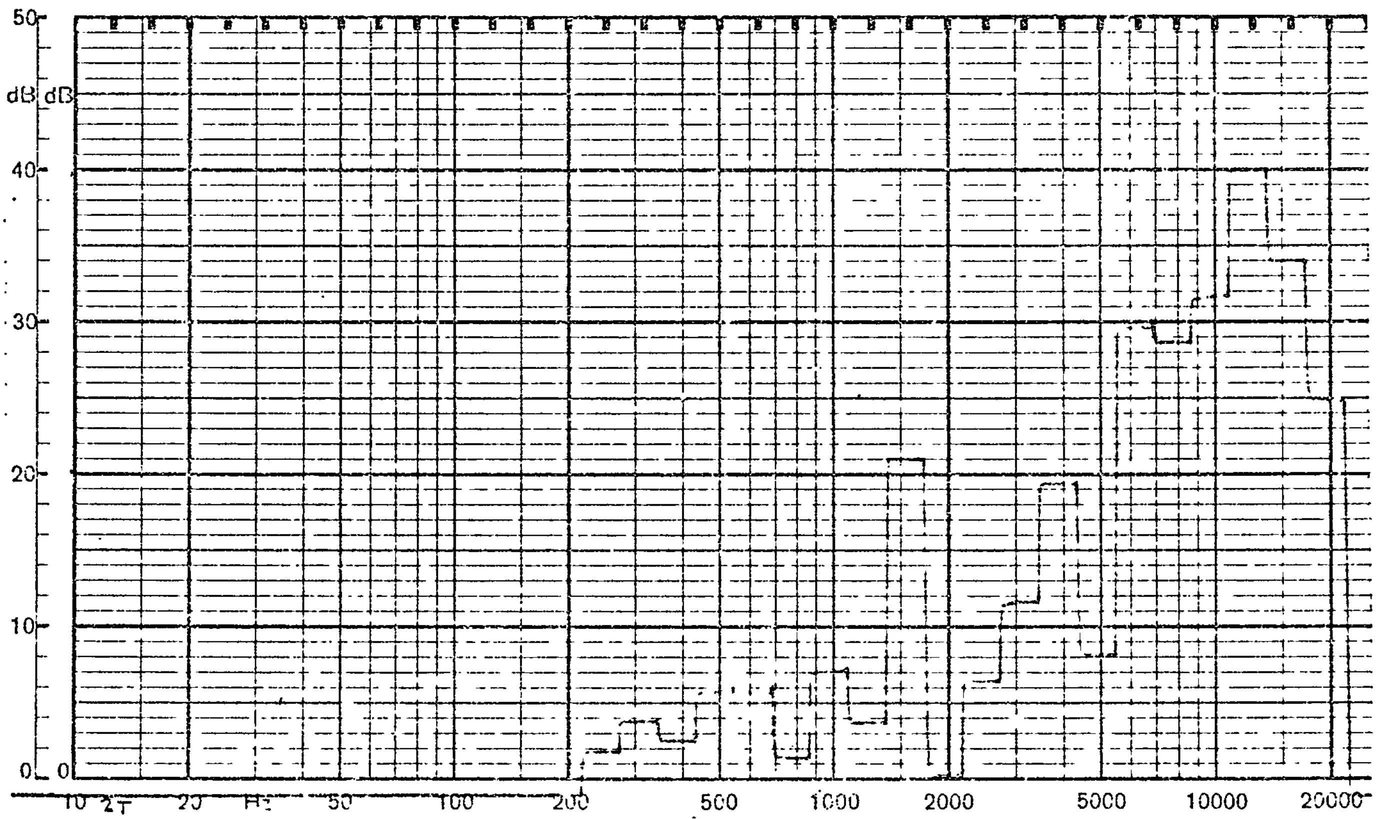

b. Wheel 2

Fig. 4.9 1/3 Octave Frequency Spectra, Impact Tests

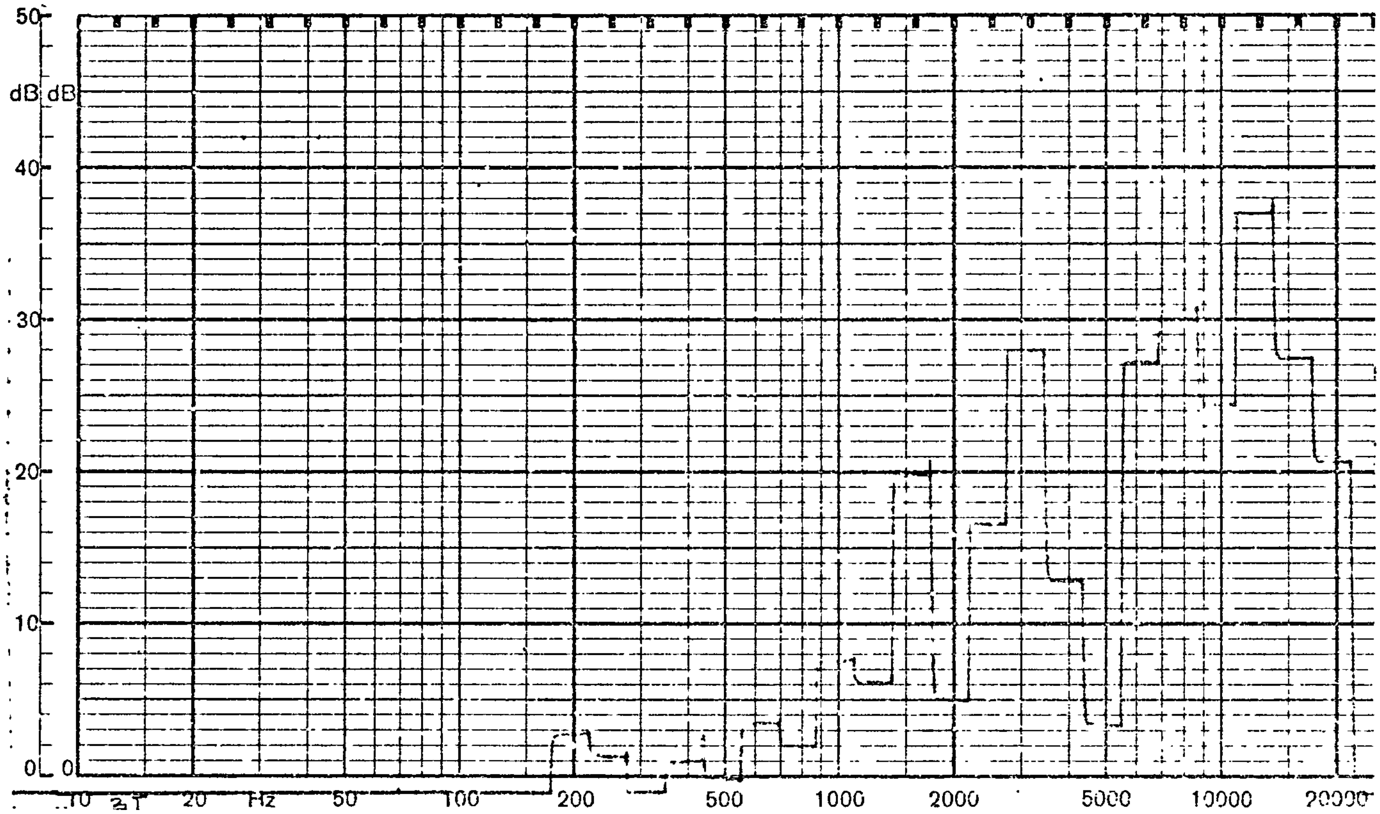

a. 1/3 Octave Frequency Spectrum for Wheel 3

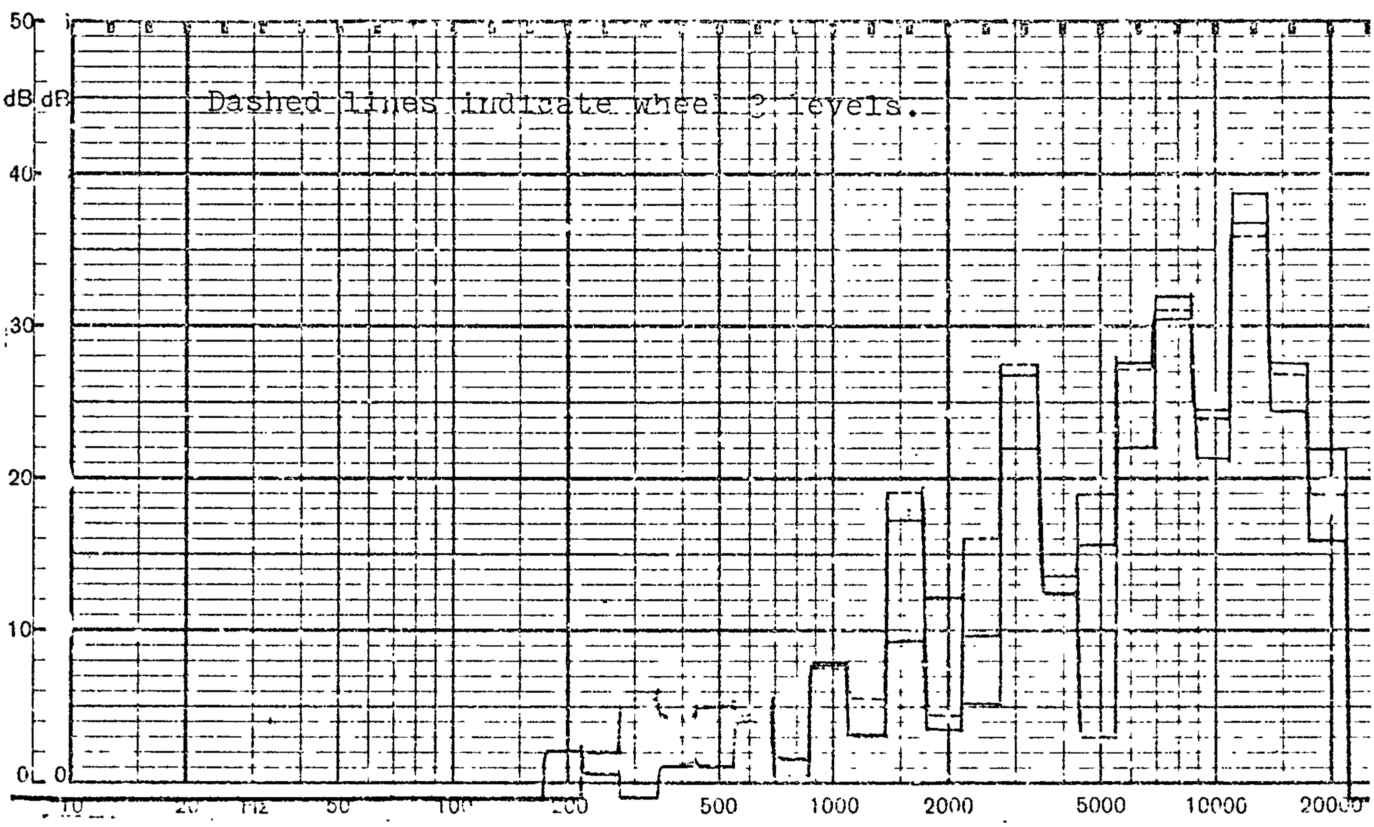

b. Comparative Graph for Wheels 1, 2 and 3

Fig. 4.10 Frequency Spectrum and Comparative Graph for Impact Tests

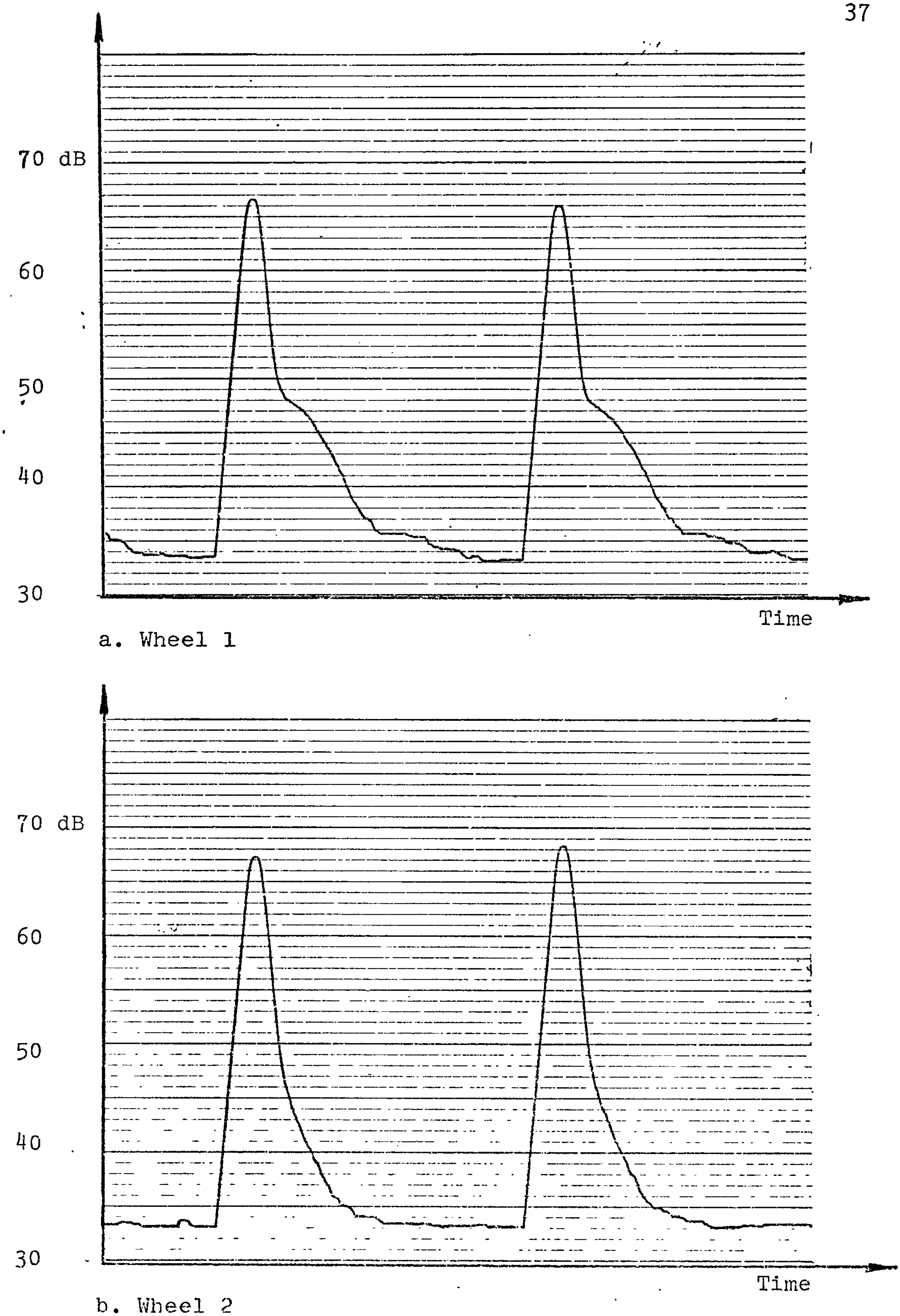

Fig. 4.11 Amplitude as a Function of Time in the 1.6 kHz Band, Impact Tests

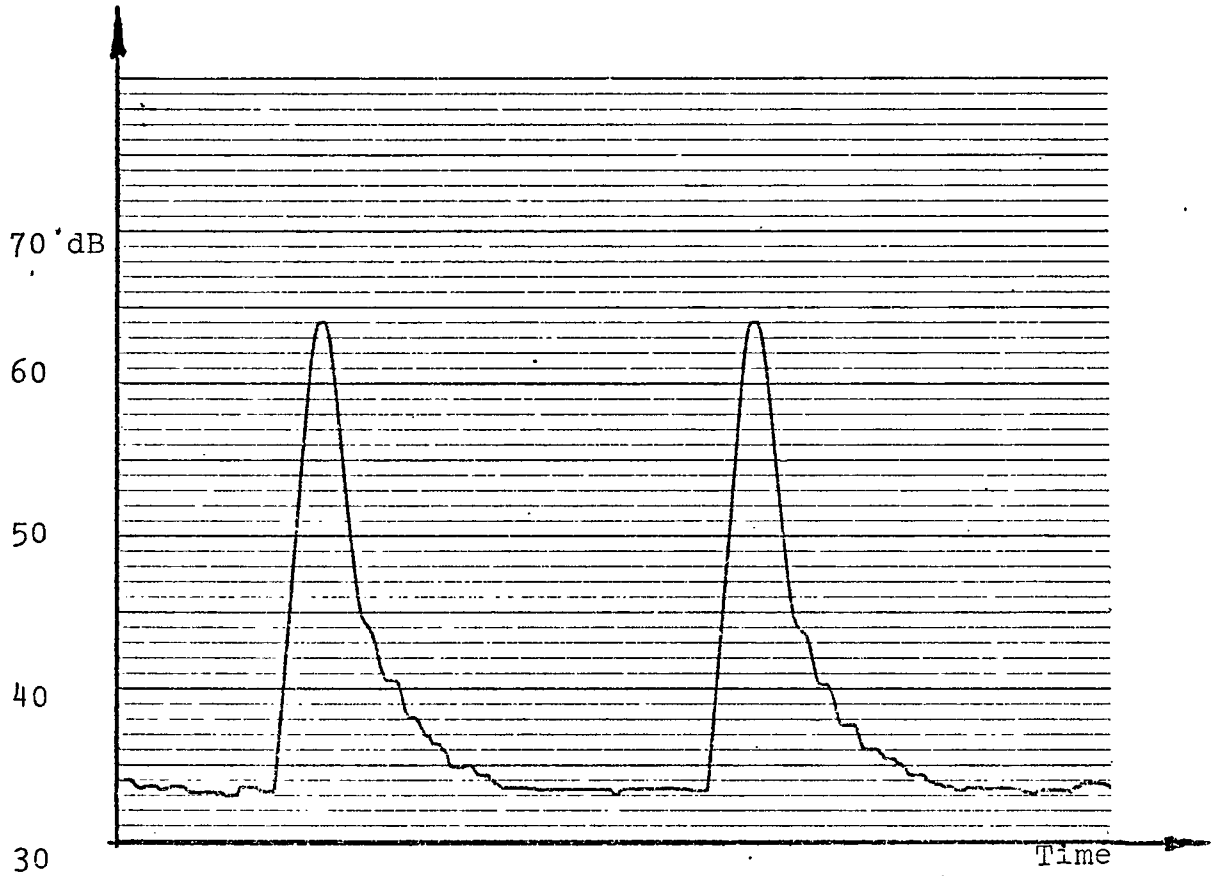

Fig. 4.12 Amplitude as a Function of Time in the 1.6 kHz Band for Wheel 3, Impact Tests

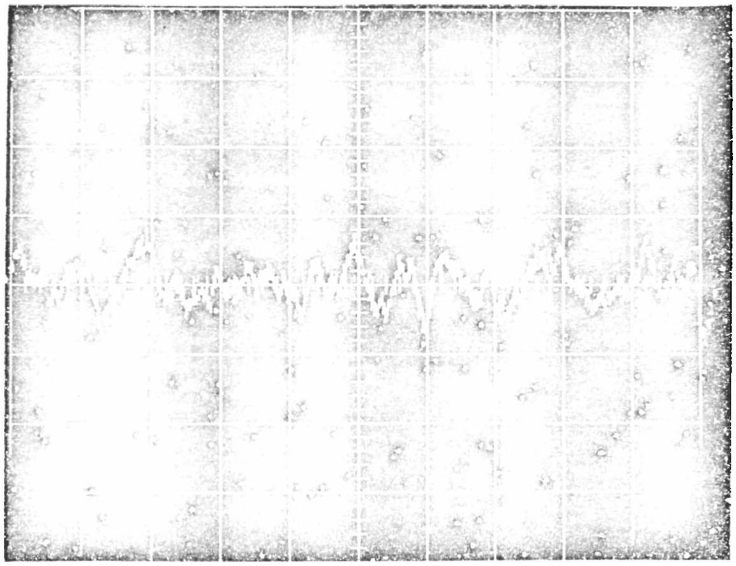

Vertical Scale 1 mv/div
Time Base 2 msec/div

a. Rolling Noise

Vertical Scale 1 mv/div
Time Base 2 msec/div

b. Impact Noise

Fig. 4.13 Oscillograms for Wheels 9 and 10 Rolling Noise Tests

Vertical Scale 1 mv/div
Time Base 2 msec/div

Fig. 4.14 Oscillogram for Wheels 9 and 10 Rubbing Noise

a. Impact Noise

b. Rubbing Noise

Fig. 4.15 1/3 Octave Frequency Spectra for Rolling Noise Tests

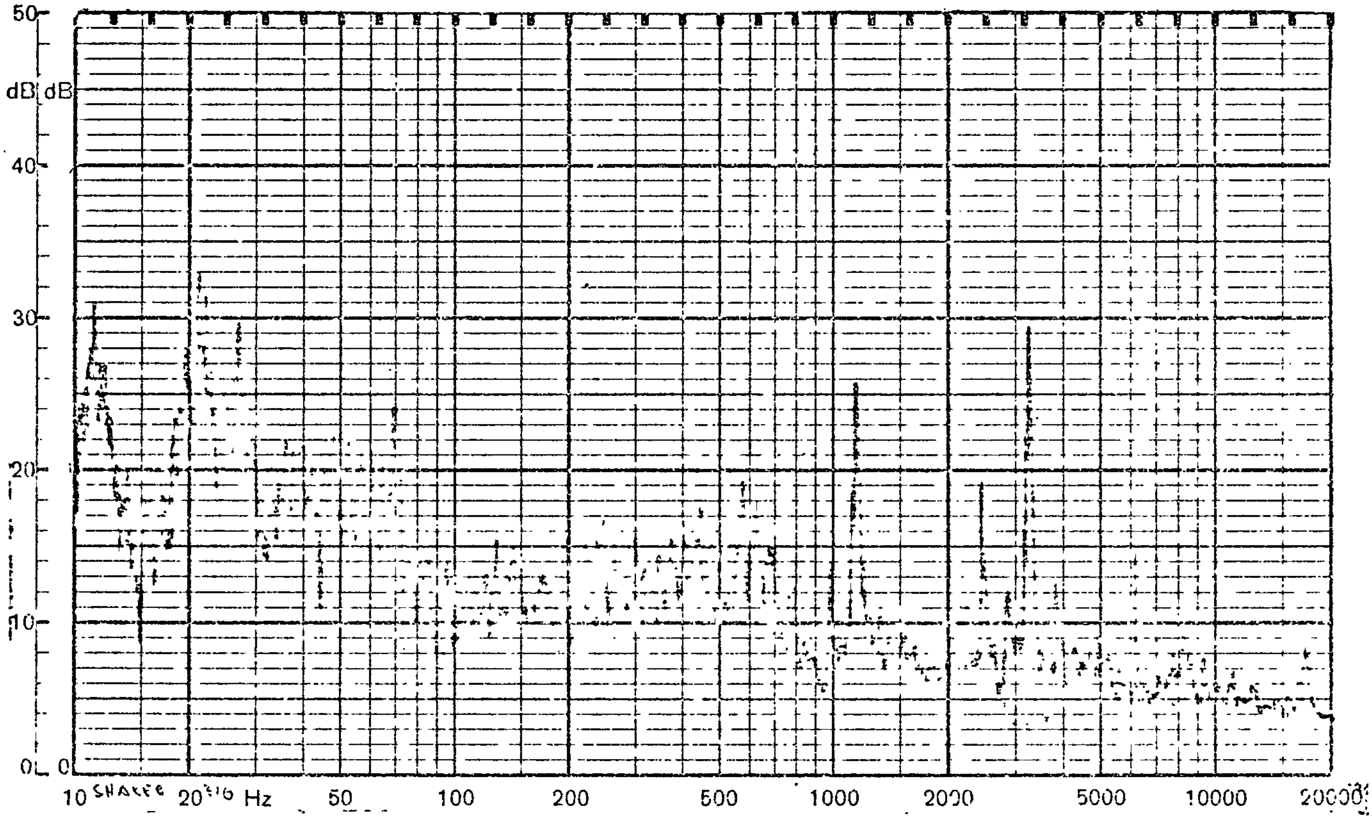

Fig. 4.16 Narrow Band Frequency Spectrum for Shaker No Load Test

Chapter 5

THEORY

5.1 Vibration of Plates

Some guidance on the vibration of a wheel can be obtained by studying the vibration of thin plates*.(see Fig. 5.1).

The following assumptions are usually made:

1. A straight line initially normal to the middle surface of the plate, will remain normal to that surface when it is deformed and unchanged in length, i.e. the transverse shear and transverse normal strains are neglected.

2. The deflections $w(x,y)$ are small compared with the thickness H of the plate.

3. The normal stresses σ_x, σ_y are zero at the middle surface of the plate.

4. For small displacements the curvatures of the middle surface may be expressed as follows:

$$\frac{1}{\rho_x} = \frac{\partial^2 w}{\partial x^2} , \tag{5.1}$$

and

$$\frac{1}{\rho_y} = \frac{\partial^2 w}{\partial y^2} . \tag{5.2}$$

The angle that the tangent plane to the middle surface makes with the x and y axes can be expressed as:

$$\phi_x \simeq \tan \phi_x = \frac{\partial w}{\partial x} ; \tag{5.3}$$

and

$$\phi_y \simeq \tan \phi_y = \frac{\partial w}{\partial y} . \tag{5.4}$$

---

* See for instance Volterra [5]

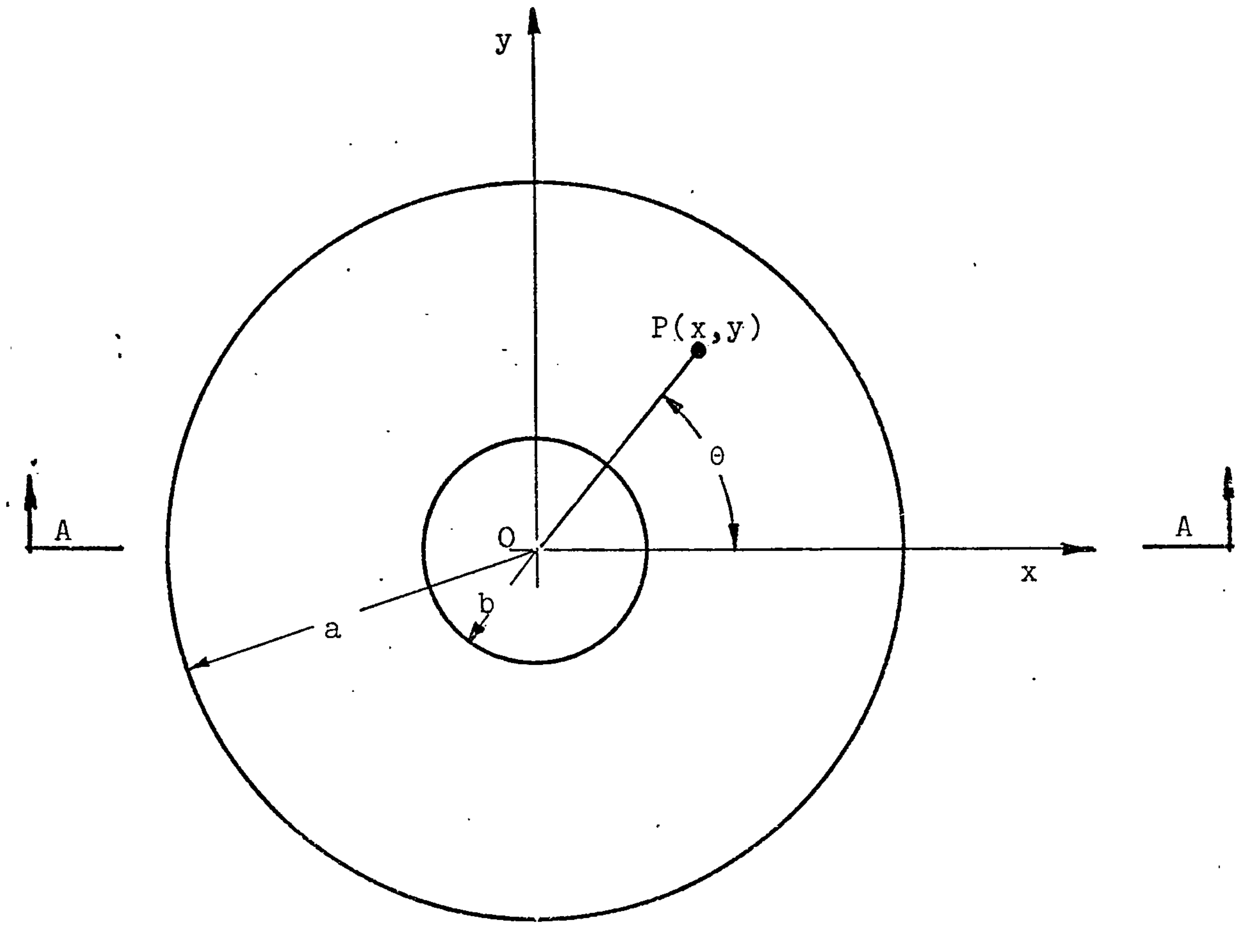

a. Annular Plate

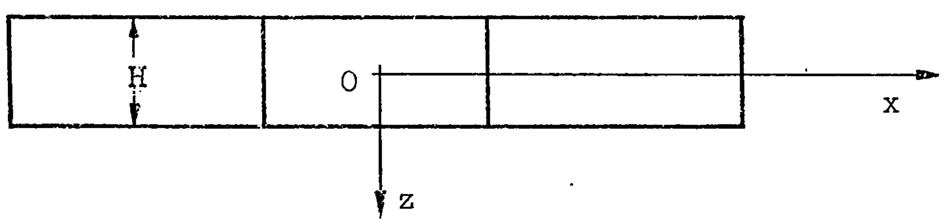

b. Section " A-A "

Fig. 5.1 Coordinate System for Annular Plate

Lagrange's equilibrium equation for a thin plate is:

$$\frac{EI}{1-\nu^2} \nabla^2\nabla^2 w = p(x,y) \tag{5.5}$$

Where p(x,y) is the external load per unit area. The equation of motion can be obtained from equation (5.5) by applying D'Alambert's principle and adding to the external force p(x,y) the "inertial force" acting on the unit area of the middle surface of the plate. The inertial force is given by

$$-\frac{\gamma}{g}H\frac{\partial^2 w}{\partial t^2} \ . \tag{5.6}$$

Combining equations (5.5) and (5.6)

$$\frac{EI}{1-\nu^2} \nabla^2\nabla^2 w = p(x,y,t)-\frac{\gamma H}{g}\frac{\partial^2 w}{\partial t^2} \tag{5.7}$$

For the case of free vibrations, equation (5.7) reduces to

$$\frac{gEI}{\gamma H(1-\nu^2)} \nabla^2\nabla^2 w=-\frac{\partial^2 w}{\partial t^2} \tag{5.8}$$

A particular solution of equation (5.8) is obtained using the method of separation of variables, assuming that

$$w(x,y,t) = W(x,y)f(t) \tag{5.9}$$

Equation (5.8) reduces to the following two equations

$$\frac{1}{f(t)}\frac{d^2 f(t)}{dt^2} = -\omega^2 \tag{5.10}$$

and

$$-\frac{\beta^2}{W(x,y)} \nabla^2\nabla^2 W(x,y) = -\omega^2, \tag{5.11}$$

where ω^2 is a constant and

$$\beta^2 = \frac{Dg}{\gamma H} = \frac{EIg}{(1-\nu^2)\gamma H}, \tag{5.12}$$

and

$$D = \frac{EI}{(1-\nu^2)} \; . \tag{5.13}$$

Rewriting equations (5.10) and (5.11) gives:

$$\frac{d^2 f(t)}{dt^2} + \omega^2 f(t) = 0 \tag{5.14}$$

and

$$\nabla^2\nabla^2 W(x,y) = \lambda^4 W(x,y), \tag{5.15}$$

where

$$\lambda = \sqrt{\frac{\omega}{\beta}} \; . \tag{5.16}$$

In polar coordinates equation (5.15) is given by:

$$\left(\frac{\partial^2}{\partial r^2}+\frac{1}{r}\frac{\partial}{\partial r}+\frac{1}{r^2}\frac{\partial^2}{\partial \theta^2}\right)\left(\frac{\partial^2 W}{\partial r^2}+\frac{1}{r}\frac{\partial W}{\partial r}+\frac{1}{r^2}\frac{\partial^2 W}{\partial \theta^2}\right)-\lambda^4 W = 0. \tag{5.17}$$

Equation (5.17) is satisfied by every solution of the following equations

$$\frac{\partial^2 W}{\partial r^2} + \frac{1}{r}\frac{\partial W}{\partial r} + \frac{1}{r^2}\frac{\partial^2 W}{\partial \theta^2} = \pm\lambda^2 W. \tag{5.18}$$

Using the method of separation of variables, let

$$W(r,\theta) = R(r)\Theta(\theta). \tag{5.19}$$

Hence the following equations are derived from equation (5.18):

$$\frac{d^2\Theta}{d\theta} + k^2\Theta = 0 \tag{5.20}$$

and

$$\frac{d^2R}{dr^2} + \frac{1}{r}\frac{dR}{dr} + \left(\pm\lambda^2 - \frac{k^2}{r^2}\right)R = 0. \tag{5.21}$$

The solution of equation (5.20) has the form:

$$\Theta(\theta) = A\cos k\theta + B\sin k\theta \tag{5.22}$$

then $\Theta(\theta)$ must be periodic and k must be an integer

$$k = n = 1,\ 2,\ 3,\ 4,\ \ldots\ldots \tag{5.23}$$

Substituting $\rho=\lambda r$ and equation (5.23) into equation (5.21) yields:

$$\frac{d^2R(\rho)}{d\rho^2} + \frac{1}{\rho}\frac{dR(\rho)}{d\rho} + \left(1 - \frac{n^2}{\rho^2}\right)R(\rho) = 0, \tag{5.24}$$

Thus the solution of equation (5.17) is:

$$\begin{aligned} W(r,\theta) = {} & [C_nJ_n(\lambda r) + D_nJ_n(i\lambda r) + E_nY_n(\lambda r) + F_nY_n(i\lambda r)] \\ & \times[A_n\cos(n\theta + B_n\sin(n\theta)] \end{aligned} \tag{5.25}$$

where J_n, Y_n are Bessel functions of order n of the first kind and second kind respectively, and C_n, D_n, E_n, F_n and λ are constants dependent on the boundary conditions.

For an annular plate with inner edge clamped and outer edge free the following boundary conditions may be assumed (see Fig. 5.2) :

a. For the outer edge

$$\frac{\partial}{\partial r}\left[\frac{\partial^2 W}{\partial r^2} + \frac{1}{r}\frac{\partial W}{\partial r} + \frac{1}{r^2}\frac{\partial^2}{\partial\theta^2}\right] + \frac{(1-\nu)}{r^2}\frac{\partial^2}{\partial\theta^2}\left[\frac{\partial W}{\partial r} - \frac{W}{r}\right]\Bigg|_{r=a} = 0 \tag{5.26}$$

and

$$\frac{1}{\nu}\frac{\partial^2 W}{\partial r^2} + \frac{1}{r}\frac{\partial W}{\partial r} + \frac{1}{r^2}\frac{\partial^2 W}{\partial\theta^2}\Bigg|_{r=a} = 0 \tag{5.27}$$

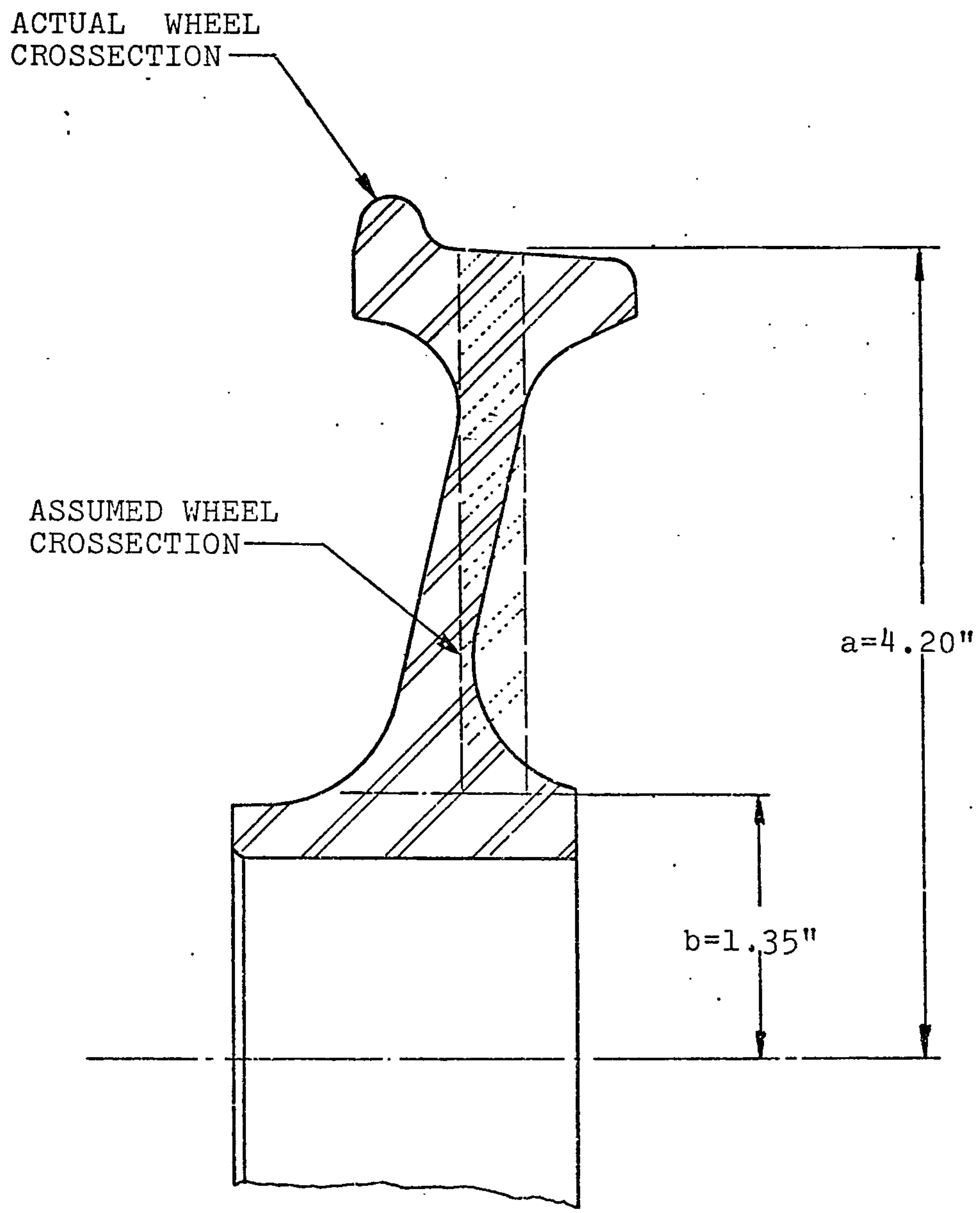

Fig. 5.2 Assumed and Actual Wheel Crossections

b. For the inner edge

$$W(b,\theta) = 0, \tag{5.28}$$

and

$$\frac{\partial W}{\partial r}(b,\theta) = 0. \tag{5.29}$$

Substituting these boundary conditions into equation (5.25) yields a frequency equation. The eigenvalues λ were computed by Southwell [26] for various ratios of b/a. Table 5.1 lists values of ($\lambda_{n,0}$ a) for n=0,1,2,3 as function of b/a. These values give the frequencies for the asymmetric modes. Poisson's ratio is assumed to be equal to 0.3 . Table 5.2 lists values of

$$\delta_{0m} = \frac{\lambda_{om}^4 a^4}{3(1-\nu^2)} \tag{5.30}$$

which yields the eigenfrequencies of the symmetric modes.

5.2 Estimation of Resonant Frequencies of a Wheel

Approximate resonant frequencies for a wheel were calculated from

$$f_{nm} = \frac{\beta}{2\pi}\lambda_{nm}^2 \qquad \text{where } n,m=0,1,2,3 \tag{5.31}$$

and the values λ were computed from constants given in Tables 5.1 and 5.2 (see Table 4.1 for list of calculated resonant frequencies).

The following assumptions were made in the calculation of these resonant frequencies:

1. The plate of the wheel is perpendicular to the axis of the wheel.

2. The plate is of constant thickness without any fillet radius at the hub or the tread.

Table 5.1 Values of $\lambda_{no}a$ for the Asymmetric Modes as a Function of b/a

b/a	$\lambda_{oo}a$	b/a	$\lambda_{1o}a$	b/a	$\lambda_{2o}a$	b/a	$\lambda_{3o}a$
0.276	2.50	0.060	1.68	0.186	2.50	0.43	4.00
0.642	5.00	0.397	3.00	0.349	3.00	0.71	5.00
0.840	9.00	0.603	4.60	0.522	4.00	0.71	7.00
		0.634	5.00	0.769	8.00	0.82	10.00
		0.771	8.00	0.81	10.00		
		0.827	11.00				

Table 5.2 Values of δ_{om} for the Symmetric Modes

m	0	1	2	3
δ_{om}	5.16	160.2	1349	5250

3. The plate is fixed at the hub (i.e. clamped at the inner radius of the annulus).

4. The plate is free at the outer edge, and the effect of the increased thickness at the rim is omitted from the analysis. This assumption may cause the largest error in the calculation of the resonant frequencies. Savin and Fleishman [7] investigated the dynamic behavior of circular plates reinforced with concentric circular ribs. Their results showed that increasing the "relative rigidity" of the rib will increase the resonant frequencies, whereas increasing the "relative mass" of the rib will cause a decrease in the resonant frequencies.

5.3 Changes in Resonant Frequencies due to In-Plane Stresses, Thermal Gradients and Presence of Cracks.

Mote [10] analysed the free vibration of centrally clamped circular saw blades by the Rayleigh-Ritz technique. He found that clamping stresses, stresses induced by centrifugal force and the presence of thermal gradients will affect the resonant frequencies. A significant result of his work is the fact that changes due to these effects are not uniform for all resonant frequencies, i.e. for the case of a centrally clamped vibrating saw blade the zeroth and first order nodal diameter resonances showed a drop in resonant frequency with increased initial stress; whereas the second order nodal diameter and higher resonances showed an increase in resonant frequencies, with increased initial stress. Similarly thermal gradients introduced at the outer edge of the saw blade altered the values of resonant frequencies. For his experiments the initial stresses were induced in the saw blades by a pair of opposing rollers which were pressed against the blade with a constant force and rolled around the circumference. Mote also found that symmetrical modes of vibration (modes with nodal lines as concentric circles) were not excited in his tests.

Sih[13] analysed the problem of elastic wave propagation around a crack. His paper considers the diffraction of compressional and vertically and horizontally polarized shear waves by a crack of finite width embedded in an infinite body. In his work he showed that the stress field around the crack is a function of Poisson's ratio, the crack geometry and the frequency of the incident waves. The intensity of the stress concentration is largest at a particular value of frequency and at a particular orientation with respect to the crack. The application of his results is limited by the fact that he assumed that the two faces of the crack are traction free. Clearly, this assumption is violated when the crack is closed by oppositely acting normal loads. Sih stated that the standing wave pattern in a vibrating body is altered by the presence of the diffracted field around a crack.

Williams[12] has shown that for a perfectly homogeneous vibrating disk the angular position of the nodal diameters depends solely on the position of the exciting force. However the presence of cracks or discontinuities eliminates the indeterminacy of position of the nodal diameters which take on preferred positions. For each mode (with at least one nodal diameter) there are two preferred nodal positions. Williams showed that a beating travelling wave component develops above a critical amplitude, when the nodal pattern disappears. He attributes this to an internal coupling force between the two preferential configurations that is due to the stretching of the neutral membrane.

Chapter 6

DISCUSSION OF RESULTS AND CONCLUSIONS

6.1 Preliminary Investigations

The initial tests for wheel 4 gave the first table of resonant frequencies obtained in the experiments. The method of excitation used resulted in additional resonances, due to the shaker support structure. It was evident from these tests that the calculated resonances were all higher than the actual resonant frequencies. As a result it was decided that a different method of support was needed for the electrodynamic shaker, in order to eliminate some of these additional resonances. Further, the suspension method for the shaker was not readily reproducible.

As repeated tests were run it soon became evident that manually sweeping the frequency band was an inadequate method to obtain the resonances. Since the sweep rate was uncontrolled some of the resonances were missed on various sweeps.

The results for wheel 9 show considerably more resonances than for wheel 4. Wheel 9 was mounted on a full axle along with wheel 10. The additional resonances were presumably due to various modes of the shaft.

6.2 Continuous Random Vibration Tests

The continuous random vibration tests were designed to eliminate the problems encountered in the preliminary investigations. The principal improvement was the use of the B&K frequency analyzer, and an improved heavy mass shaker mount. On repeated tests for a particular wheel the amplitude of the resonances stayed within ± 1 dB.

The theoretical analysis was too approximate to provide accurate values for the resonant frequencies. Thus it was decided that comparative tests were needed to obtain differences between good and cracked wheels. Narrow band (3.16 Hz bandwidth) frequency spectra were obtained for wheels 1 through 8. It was expected that wheels 7 and 8 (both with artificial cracks) would have similar spectra while wheel 6 (a good wheel) would be different. The results show that there are significant differences in the spectrum between wheel 6 and wheels 7 and 8, but differences may be due to the lack of uniformity in the method used to shrink fit the wheels onto the stub axles rather than presence of the artificial crack. Different initial stress levels may have caused the changes in the spectrum, as Mote [10] showed to be the case for circular saw blades. It must be noted that the Wheel and Axle Manual [15] of the Association of American Railroads prescribes uniform wheel press practice, so this should not be a problem in practice.

To overcome the shrink fit problem wheels 1, 2 and 3 were selected for testing from the unmounted wheels. These wheels were alike in all respects except for a machined crack in the plate of wheel 3. The results obtained from these wheels were consistent when excited with a 50 kHz randomly varying force input. The analysed responses showed:

1. The spectra obtained with a 3.16 Hz bandwidth tracking filter always showed a 50 to 100 Hz downward shift in the

resonances of wheel 3 at 1.7, 3, 7.2 and 12 Hz. The amplitudes at resonance were never consistent enough to be used for discriminating between good or bad wheels. The sweep rate of this method of analysis is 5 to 10 minutes (depending on chart speed setting of the instrument) thus the potential applications to non destructive testing are somewhat limited when a large number of wheels are to be inspected.

2. The real time 1/3 octave analyzer provided repeatable 1/3 octave frequency spectra for wheels 1, 2 and 3. The amplitude difference between wheels 1 and 2 was less than 2 dB at all bands except at the 6.3 kHz centerfrequency band where it was 4 to 7 dB. Wheel 3 however differed from 1 and 2 in six bands consistently by at least 4 to 7 dB. This method of analysis is the most reliable, since it is fast (30 seconds at a maximum) and the differences are repeatable.

3. The spectra that were obtained with 10, 31.6, 100 Hz bandwidth filters produced results quite similar to those obtained with the 3.16 Hz bandwidth filters. There was a consistent downward shift at some of the resonances for wheel 3.

6.3 Continuous Sine Wave Sweep Tests

Continuous sine wave sweeps did not show sufficient differences between good and cracked wheels to show any promise for future non destructive testing applications. It is possible that slower sweeprates, than were used for this experiment might give better results.

6.4 Impact Tests

The comparative 1/3 octave band graphs for wheels 1, 2 and

3 did not produce consistent differences that might be used to find cracked wheels using the impact technique. This may have been due to the fact that accurate jigs were not employed to locate the wheel the same distance from the shaker for successive test runs. The hammer that was attached to the shaker accelerated over a path of variable length, and thus delivered a force that varied in magnitude.

Schroeer, Rowand and Kamm [14] carried out an extensive test program using an electrodynamic impacter and accelerometer pickups. They tested a variety of structural components (riveted aluminum panels, honeycomb panels, laminated panels and turbine disks). In their tests they used accurate jigs to position the part for each test run. They found that the test results deteriorated with increased error in positioning the part from the impacter. Their tests however showed that the impact technique indeed is suitable for crack detection. They fatigued flat metal bars (7 1/2" x 2" x 1/8") and produced cracks of varying lengths. The amplitude of the accelerometer reading was inversely proportional to the size of crack in the frequency range 5 to 15 kHz.

The impact tests performed by this author produced a beating effect in wheel 3. This effect was present only for large amplitude vibration. This may be an example of the phenomenon described by Williams (see Chapter 5). Schroeer, Rowand and Kamm encountered this beating effect but they assumed that it was due to the presence of some holes and slots in the periphery of their disk. They still noted however that the maximum amplitude of the signal strength varied according to the degree of fatigue in the disk. The presence of the beating effect requires further investigation before its usefulness as a nondestructive testing criteria can be asserted.

6.5 Rolling Noise Tests

The rolling noise tests established that slow speed rolling and impact of an unloaded wheel and axle set on the track is not sufficient to excite the resonant frequencies of the wheels. However it was shown that when the flange of the wheel contacts the rail while rolling there results an intense sound. A wheel rolling around a sharp curve produces such a noise in practice.

6.6 Summary

These experiments showed that:

1. Wheels with cracks can be detected by the analysis of the airborne sound that is emitted from the wheel (when the wheel resonances are suitably excited).

2. The method of detection is on a comparative basis by matching the resonances of good wheels against the resonances of the wheel under test.

3. For stationary tests wide band (50 kHz bandwidth) random noise excitation gives better comparative results than impact excitation.

4. Real time 1/3 octave analysis proved adequate to discriminate between cracked and good wheels.

Chapter 7

SUGGESTIONS FOR FURTHER WORK

The investigations performed for this thesis were only for 1/4 scale model railway wheels. While they yielded encouraging results, the need is obvious for an extensive test program with full size railroad wheels, with particular attention to the following points:

1. Investigation of the behavior of good full size wheels under various modes of excitation.
2. Experimental and theoretical analysis of the spectral response of wheels of different size, manufacture and age.
3. Investigation of the response of railway wheels with different types of wheel failures that are encountered in railroad service.

Appendix 1

MANUFACTURE OF ARTIFICIAL CRACKS IN WHEELS

For wheels 3, 7 and 8 artificial cracks were machined on an electro discharge machine. An electrode was made of the same dimensions as the desired crack size (see Figure A1.1) In the electro discharge process the wheel and the electrode are securely clamped in the machine fixtures. An electrolyte bath completely surrounds the electrode and the wheel. A current is then passed through them. At the wheel and electrode interface arcing takes place removing small quantities of wheel material. The electrode is mechanically advanced to the desired depth at the same rate at which the wheel material is removed.

An attempt was made to obtain artificial cracks in wheel 5 by heating the wheel locally with a acetylene torch and quenching the hot wheel in water bath. This method produced small cracks in the tread and the flange of wheel 5. This method locally hardened the wheel; thus wheel 5 can not be considered as a good facsimile of full size railroad wheels.

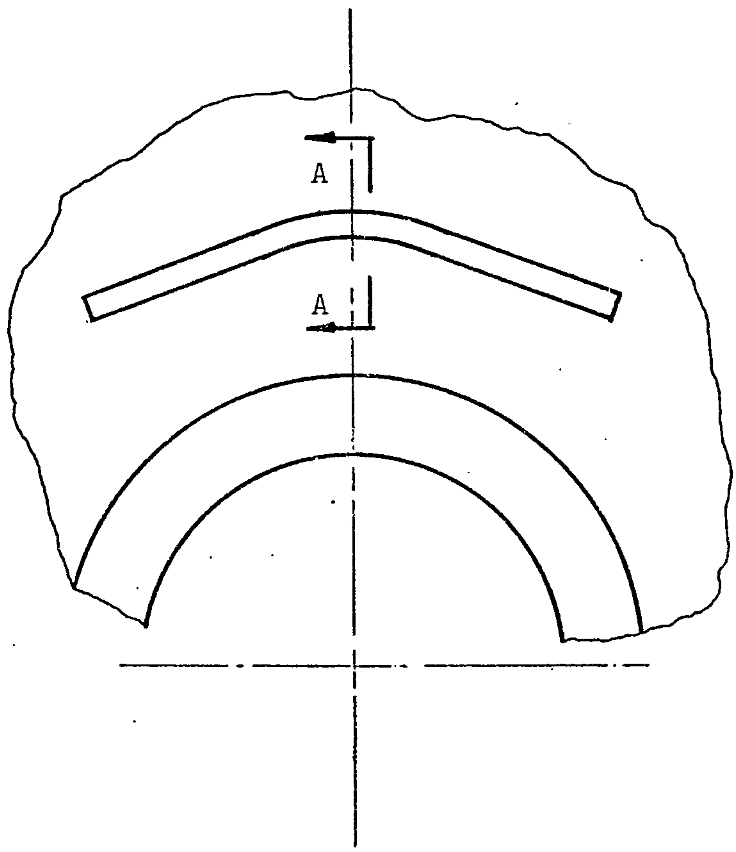

a. View of Crack in Plate

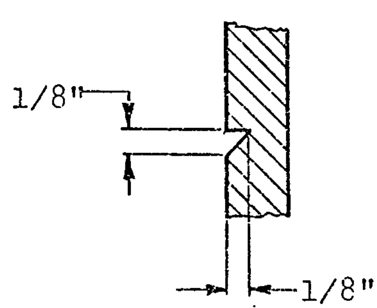

b. Section "A-A"

Fig. A1.1 Detail of Crack in Plate of Wheel 3

Appendix 2

EQUIPMENT LIST

Storage Oscilloscope, Tektronix, Type 564

Spectrum Analyzer Unit, Tektronix, Type 3L5

Time Base Unit, Tektronix, Type 2B67

Storage Oscilloscope, Tektronix, Type 564B

Four Trace Amplifier Unit, Tektronix, Type 3A74

Time Base Unit, Tektronix, Type 3B4

Oscilloscope Camera, Hewlett Packard, Model 196A

Film, Polaroid Land, Type 47

Random Noise Voltmeter, Bruel & Kjaer, Type 2417

Electronic Counter, Hewlett Packard, Model 523 DR

Regulated DC Power Supply, Kepco, Model CK 36-1.5

2 Variable Band-Pass Filters, Krohn-Hite, Model 310 CR

Variable Band-Pass Filter, Spencer-Kennedy Labs., Model 302

Decade Amplifiers, H. H. Scott, Type 140B

Power Oscillator/Amplifiers, Ling, Model POA-1

2 Random Noise Generators, General Radio, Type 1381

DC Power Supply, Endevco, Model 2622

4 Subminiature AC Accelerometer Amplifiers, Endevco, Model 2607

2 Micro-Miniature Shear Accelerometer, Endevco, Model 2226C

Real Time Third Octave Analyzer, Bruel & Kjaer, Type 3347

Sine Random Generator, Bruel & Kjaer, Type 1024

Measuring Amplifier, Bruel & Kjaer, Type 2606

Heterodyne Slave Filter, Bruel & Kjaer, Type 2020

Level Recorder, Bruel & Kjaer, Type 2305

BIBLIOGRAPHY

[1] Bray, D. E., Pulse Excitation of Railway Wheels, M. S. Thesis, University of Houston, 1969.

[2] Dalvi, N. G., Detection of Thermal Cracks in Railway Wheels Using Ultrasonic Surface Waves. M.S. Thesis, University Of Houston, 1970

[3] Bray, D. E., Private Communication, 1971 .

[4] Timoshenko, S., Vibration Problems in Engineering, D. Van Nostrand Co., Inc., New York, 1955.

[5] Volterra, E., Dynamics of Vibrations, Charles E. Merrill Books, Inc., Columbus, Ohio,1965.

[6] Leissa,A. W.,"Vibration of Plates," NASA SP-160, 1969.

[7] Savin, G. N., Fleishman, N. P., "Rib-Reinforced Plates and Shells," NASA TT F-427, 1967.

[8] Harris, C. M., Crede, C. E., Shock and Vibration Handbook, McGraw-Hill Book Company, New York, 1961.

[9] Crenwelge, O. E.,Jr., Simulation with Minimum Equipment of Random Vibration Induced by Complex Excitation, Ph.D. Dissertation, University of Houston, 1970.

[10] Mote, C. D.,Jr., "Free Vibration of Initially Stressed Circular Disks," ASME Paper No. 64 - WA/MD - 4., 1964.

[11] Kirschner, F., "Control of Railroad Wheel Screech Noise," The Soundcoat Company, Inc., 1968.

[12] Williams, C. J. H.,"The Stability of Nodal Patterns in Disk Vibration," Int. J. Mech. Sci. Pergamon Press Ltd., 1966.

[13] Sih, G. C., "Propagation of Elastic Waves Around a Crack," Presented at the Third Conference of the Hungarian Academy of Sciences on Diminsioning and Strength Calculations in Budapest, Hungary, October 1968.

[14] Schroeer, R., Rowand, R., Kamm, H., "The Acoustic Impact Technique, a Versatile Tool for Nondestructive Evaluation of Aerospace Structures and Components," Presented at the 1970 Spring Conference of the American Society for Nondestructive Testing in Los Angeles.

[15] Association of American Railroads, Wheel and Axle Manual, Ninth Edition, 1968.

[16] Graff, W. J., Underwood, A. C., "Machinery Noise May Indicate Loss of Efficiency and Severity of Dynamic Stresses," ASME Paper No. 70-WA/Pet-2, 1970.

[17] Elson, B. M., "Optical System Analyzes Engines," Aviation Week & Space Technology, March 1, 1971.

[18] Yontar, M., "Research on the Operating Stresses in Path Railcar Axles, Drive Systems, Wheels, and Rail Joints," ASME Paper No. 66-RR-6, 1966.

[19] Thomson, W. T., Vibration Theory and Applications, Prentice-Hall, Inc., Englewood Cliffs, N.J., 1965.

[20] Stephens, R. W. B., Bate, A. E., Acoustics and Vibrational Physics, Edward Arnold LTD., London, 1966.

[21] Peterson, A. P. G., Gross, E. E., Jr., Handbook of Noise Measurement, General Radio Company, West Concord, Massachusetts, 1967.

[22] Zienkiewic, O, C., Cheung, Y. K., The Finite Element Method in Structural and Continuum Mechanics, McGraw-Hill Publishing Company Limited, New York, 1967.

[23] Wah, T., Calcote, L. R., Structural Analysis by Finite Difference Calculus, Van Nostrand Reinhold Company, New York, 1970.

[24] Meirovitch, L., Analytical Methods in Vibrations, The MacMillan Company, New York, 1967.

[25] Lindsay, R. B., Mechanical Radiation, McGraw-Hill Book Company, New York, 1960.

[26] Southwell, R. V., " On the Free Transverse Vibrations of a Uniform Circular Disc Clamped at its Center and on the Effects of Rotation," Proceedings of the London Royal Society, Series A, Vol. CI, 1922,pp. 133-53.